



MAX-PLANCK-GESELLSCHAFT



## Part B

### 2.1. Ammonia Synthesis

Prof. Dr. R. Schlögl

Department of Inorganic Chemistry, Fritz-Haber-Institute of the MPG,  
Faradayweg 4-6, 14195 Berlin, Germany

Corresponding author: e-mail [schloegl@fhi-berlin.mpg.de](mailto:schloegl@fhi-berlin.mpg.de),  
phone +49 30 8413 4400, fax +49 30 8413 4401

#### Contents

- 2.1.1. Introduction
- 2.1.2. Some basic considerations
  - 2.1.2.1. Concepts
  - 2.1.2.2. Choice of the catalyst
- 2.1.3. Thermodynamic aspects
  - 2.1.3.1. Dinitrogen
  - 2.1.3.2. Nitrides
  - 2.1.3.3. Hydrogen
  - 2.1.3.4. The reaction
  - 2.1.3.5. Phase diagrams
- 2.1.4. Generation and structure of „ammonia iron“
  - 2.1.4.1. Some reference experiments
  - 2.1.4.2. The structure of the oxide precursor
  - 2.1.4.3. The activation process
  - 2.1.4.4. Microtexture of the activated catalyst
  - 2.1.4.5. Microstructure of the activated catalyst
  - 2.1.4.6. Summary: The nature of the iron catalyst
- 2.1.5. The single crystal approach to ammonia synthesis
  - 2.1.5.1. Single crystal structures
  - 2.1.5.2. Energetics of chemisorption of hydrogen and nitrogen
  - 2.1.5.3. Structure and energetics of chemisorbed ammonia
  - 2.1.5.4. Kinetics of nitrogen chemisorption

- 2.1.5.5. The effect of the potassium promoter
- 2.1.6. Nitrogen chemisorption with polycrystalline substrates and at elevated pressures
  - 2.1.6.1. Model studies
  - 2.1.6.2. Polycrystalline substrates
- 2.1.7. The mechanism of ammonia synthesis
  - 2.1.7.1. Basic kinetic information
  - 2.1.7.2. Analytical rate equations
  - 2.1.7.3. Microkinetic rate equations
- 2.1.8. Conclusion

## 2.1.1 Introduction

The catalytic synthesis of ammonia is one of mankind largest synthetic chemical reactions. It is of strategic importance since it is the key to nitrogen chemistry. All other nitrogen-atoms containing chemicals are synthesised from ammonia. Nitrogen containing molecules are required for several general purposes:

\* Instantaneous release of the chemical energy stored in the separated N-N triple bond: explosives and propellants

\* Use of the affinity of molecules containing nitrogen in different formal oxidation states to couple and to form e.g. a chromophoric electron system: dyestuffs

\* Use of the basicity of the nitrogen atom lone pair: amino compounds, nitrogen heterocyclic functional molecules, fertilisers and biosynthetic applications.

The supply of ammonia required for these branches of chemistry is generated from air and fossil fuels, today mostly natural gas or from petrochemical products. The synthesis of ammonia in integrated plants is so perfectionised today that the cost of ammonia is to a large extent given by the energy cost of the fossil fuel. This sets a limit for possible improvements by the catalytic science of ammonia synthesis.

Another strategic relevance of ammonia synthesis is its use as „bellwether reaction“ [1] or „drosophila reaction“ in catalysis science. Most conceptual developments in catalysis science were tested with the ammonia synthesis reaction which can be considered as the best understood catalytic process. This is reflected in the enormous body of literature which was recently collected in several monographs.

*Catalytic Ammonia Synthesis*

*Editor: J.R. Jennings, Plenum 1991*

*M. Grunze, in:*

*The Chemistry and Physics of Solid Surfaces and Heterogeneous Catalysis*

*Editors: D. A. King, D. P. Woodruff, Elsevier, 1982, Vol. 4*

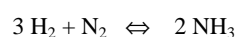
*A. Nielsen: Ammonia Synthesis*

*Springer 1995*

These references are characterised for the benefit of the reader as follows: The first book deals primarily with the catalysis science including surface science, kinetics and solid state chemistry and reviews the history of ammonia synthesis as well as further possible developments, in particular for non-iron catalyst systems. The second review deals exclusively with the details of the fundamental surface science of ammonia synthesis on well-defined iron substrates. The book of the third reference aims at a complete referencing of the relevant literature and contains a complete account on the technology of ammonia synthesis including engineering kinetics and plant design. The fundamental science chapters present one picture of the process and contain less factual material than the first book which in turn is much less complete in coverage of the literature. These comments are biased by the author but may help the reader to consult the most relevant review source as the present article does not intend to cover all literature as well as it aims not at a reconstruction of the historic development of our present understanding. The present article tries to give a picture of today's understanding of this reaction from the point of view of a chemist interested in the mechanism at an atomic level and in the solid state chemistry of the extremely successful catalyst system.

## 2.1.2 Some basic considerations

At a first glance, the reaction of two main group elements to a small molecule has little spectacular.



There are two principal reaction pathways how the ammonia can be formed. Common to both is the activation of molecular hydrogen into the reducing agent atomic hydrogen and some kind of activation of the nitrogen molecule. The difference lies in the choice of the nitrogen molecule dissociation step to occur before hydrogenation of atomic nitrogen or after partial hydrogenation to diimine and hydrazine. In the most efficient biological nitrogen fixation systems the molecular approach is observed [2] whereas the technical reaction proceeds via the atomic nitrogen route [3, 4].

The inorganic catalyst has thus to accomplish two functions, namely to activate molecular hydrogen and to activate molecular nitrogen. The activity for both reactions, on the other hand, has to be moderate enough not to decompose the product ammonia faster into its atomic constituents than its formation occurs. Another boundary condition for the choice of a catalyst is to avoid the chemical reaction of atomic hydrogen or atomic nitrogen with the catalyst to stable hydrides or nitrides. This would self-poison the catalyst in the same way as strong chemisorption of the Lewis base ammonia on a Lewis acid catalyst surface. In this context it is pointed out that ammonia and its atomic constituents provide a relevant virtual pressure [5] which is significantly higher than its corresponding hydrostatic pressure allowing thus for the formation of hydrides or nitrides which would be assumed to be metastable from normal phase diagrams. The example of ammonia synthesis over metallic iron forms a drastic example for the operation of the virtual pressure effect as quantitatively shown in [6].

The choice of the catalyst requires thus a system which provides free electrons to activate the molecular constituents. This activation by electron transfer has to be moderate enough to create *reactive* atomic species. Chemically speaking, neither strongly Lewis acidic systems such as Ti or Mo nor strongly basic systems such as Ni, Pt are good candidates and the found optimum of iron and ruthenium is no surprise following these general ideas. It should be pointed out that such estimates were done using thermodynamic data [7] but it should also be noted that these estimations occurred after the good catalysts were found by Mittasch empirically (see below). Recently, the same chemical trend rules were used to interpret the conclusion from a quantum chemical treatment of the choice of the ideal catalyst that the best catalysts are those with an intermediate number of d-electrons in the valence band [8].

In the situation having to optimise two different reactions it is useful to estimate the relative ease of their progress which is done to a first approximation by looking

at the thermodynamic boundary conditions of the reaction (see section 2.1.3). It is apparent that the activation of nitrogen is the most difficult step. This process is now understood in many of its details (see below) thanks to the surface science approach targeting at a study of each elementary step required for the whole reaction from gaseous molecular nitrogen to reactive atomic nitrogen. The activation of molecular hydrogen is easier to accomplish leading to a situation in which the catalyst may be covered with hydrogen atoms in large excess over nitrogen atoms. If hydrogen is bonded too strongly to the catalyst a self-poisoning reaction may occur similar to the case of hydride or nitride formation.

Unfortunately, there are several impurity species such as water, oxygen or carbon monoxide which are even more easily activated than hydrogen and which bond firmly to the catalyst surface. These common impurities of the gas feed act thus as poisons of the catalyst and must be avoided to an extent that the gas feed is pure to a sub-ppm level in modern plants. The preparation of the gas feed is a major part of the technical ammonia synthesis process requiring a significantly larger fraction of the equipment than the synthesis step itself. The development of catalysts which are significantly more tolerant to impurities than the present systems provides a potential for a simpler overall synthesis plant.

The analysis of the ammonia synthesis process in its mechanistic details is even more complicated as technical catalysts consist not only of a transition metal element but contain small amounts of desired impurities of main group element oxides which act as promoters and enhance the performance of the catalyst significantly. This enhancement is so significant that it is not possible to separate the catalyst in a pure system and a promoted system. The presence of the promoters as well as a special fusion process of the precursor oxide material create a unique form of the transition metal iron which is the active component in most industrial systems today. For the single crystal approach [9] special orientations of the model surface have to be chosen and surface preparations have to be performed before any sustained activity can be obtained. This shows that ammonia synthesis is a structure-sensitive reaction occurring not on any form of iron metal. It will be described how this fundamental result of surface science is reflected in the preparation of the technical catalyst. It has to be pointed out that the technology existed much earlier than its scientific foundation.

The application of ruthenium catalysts which are intrinsically highly active in technical systems [10] requires a support of the active metal onto an inert substrate and keeping it in high dispersion under synthesis conditions.

The price of the metal and its physical properties do not permit its application as a fused catalyst system with a low surface area. Significant scientific [11,12] and technological efforts [10] brought about a system competitive to the iron technology using Ru on carbon supported catalysts. The mode of operation and its promotion by alkali metals contain still scientific puzzles, similar to the situation for the iron system about 25 years ago.

### 2.1..2.1 Ammonia Synthesis as Reference Reaction in Catalysis Science

In a recent review [1] it was pointed out why ammonia synthesis is of so eminent importance for catalysis science: all general concepts of catalysis were developed and formulated in relation to ammonia synthesis. This is not only a consequence of the historical impact and the enormous practical importance of the reaction, but also because of the apparent simplicity of the process. There is no selectivity problem, the catalyst is conceptually simple as a pure metallic element seems to be the adequate model system for the technical catalyst. The reaction can be operated under conditions ranging from equilibrium and near-equilibrium situations up to conditions very far from equilibrium at low pressures and temperatures. In addition, the reaction can be conveniently studied in both directions, i.e. formation and decomposition of ammonia can be observed with comparatively little experimental problems.

The first concept is that of the **rate determining step (rds)**. It implies that in a catalytic cycle of several elementary steps one step is not in thermodynamic equilibrium which determines with its individual reaction rates the overall rate equation for the conversion. In ammonia synthesis this step is the adsorption of nitrogen [5] which may be referred to better as the activation of nitrogen. In ammonia decomposition this step is the recombinative desorption of di-nitrogen from the surface. The experimental technique of isotope labelling of one educt and observation of its occurrence in the product under equilibrium reaction conditions was designed [13] to identify the *rds* in ammonia synthesis. It is noted that the nature of the *rds* may change with the external reaction conditions, a fact which has led to significant controversies in the past. A discussion of this point in general terms can be found in [14].

Related to this concept is the definition of the **most abundant reactive intermediate (mari)**. A single atomic or molecular species present on the catalyst determines by its steady state abundance the overall kinetics of the process. This *mari* is in many cases not

known with its exact atomic arrangement but occurs as a „joker“ species such as „chemisorbed nitrogen“ in the rate equation formalisms.

A central concept in catalysis is the unambiguous definition of „activity“. For this purpose the concept of **turnover frequency (tof)** was defined [15, 13]. The quantity describes the number of catalytic cycles per active site and time. Its definition implies the concept of active sites as well-defined and countable surface structural elements on a catalyst. This has been illustrated for iron supported particles in ammonia synthesis in a combined structural and kinetic study [16] and large variations of the *tof* with particle size from 1000 to 35.000 s<sup>-1</sup> have been found. The particle size was determined by a combination of physical and chemisorption techniques yielding good numerical agreement. The following table lists the results.

Table 1. Ammonia synthesis with iron/MgO supported model catalysts

Loading % Fe	Particle size (nm)	Particle surface area (nm <sup>2</sup> )	Turnover frequenc y * (s <sup>-1</sup> )	Turnover per unit surface area (nm <sup>-2</sup> s <sup>-1</sup> )
1.0	1.5	7.06	1000	142
5.0	4.0	50.24	9000	179
40.0	30.0	2825	35.000	12

\* 678 K, stoichiometric mixture, 1 atm total pressure

The data for the *tof* were here determined under conditions of pure kinetic control allowing to reflect true properties of the catalyst samples. The *tof* increases with particle diameter which was taken as indication for the **structure sensitivity** of ammonia synthesis [17], another concept in catalysis meaning that the activity (or *tof*) of a reaction will be dependent on the surface crystallographic structure of the catalyst. Underlying is the principle that on different particles or crystal face orientations different local geometries of active sites or different site densities will be found. This follows evidently from the *tof* per unit surface area (for the simplistic case of spherical particles) shown in

table 1. The large particles contain either less-active catalytic centres or a smaller number per unit surface area of the same active centres than found on the small particles. As the physical characterisations gave no hints on principal differences of the surfaces of the three samples the assumption of a smaller site density seems adequate. This assumption clashes, on the other side, with the fundamental concept of a **heterogeneous site distribution** which has to be assumed for the derivation of the formal kinetic description of ammonia synthesis according to the Temkin approach. The case serves as example for the problems which are encountered in catalysis science with defining such a conceptually simple quantity as „activity“.

Ammonia synthesis is also one prototype example [18] for the current strategy in catalysis science referred to as the „single crystal approach“ [9]. This approach requires first a solid knowledge of the working catalyst surface constitution and information on the mode of action of each constituent of this surface. Based on this information a simplified single crystal surface of suitable size can be prepared and all elementary reactions of the catalytic cycle can be studied qualitatively and quantitatively. On the basis of this set of data set a microkinetic model containing the elementary step parameters from the single crystal data can be set up which ultimately will allow to describe the behaviour of a catalyst under technical reaction conditions without having to assume unique surface chemistry or even having to use model parameters without known physical meaning. All this was accomplished for ammonia synthesis. Although some details of the procedure are still under debate this reaction is the first worked example of a completed suite of experiments and theoretical evaluations to understand successfully a technical catalytic process. The present article is intended to supply the currently available information for each step of this procedure in order to allow the reader to estimate the physical validity of the final result of the whole procedure displayed in Figure 1.

In this Figure the correlation is illustrated between a theoretical prediction and actual measurements of the performance of an ammonia synthesis catalyst over a wide range of total pressure. Although the scale is double logarithmic this result is seen [18] as a major breakthrough in catalysis science. This success was only possible through the co-operation of several scientific and engineering disciplines highlighting the interdisciplinary character of targeted catalysis science.

### 2.1.2.2. Choice of the catalyst system

In the course of the history of ammonia synthesis a large number of catalysts systems were tested. Many of them proved to be active systems but only two systems are of practical relevance. The by far most important is promoted elemental iron prepared in a special reduction procedure from promoted fused iron oxides. The other system is promoted elemental ruthenium in dispersed form. Both systems will be covered in this article but following the available literature a strong emphasis will be placed on the iron system.

For a historic description of how iron was discovered as ammonia catalyst see the literature of A. Mittasch, the inventor of the present catalyst system [19,20]. Iron was first used by A. B. Berthollet in 1808 and subsequently by W. Ostwald (1900) and F. Haber (1904) for their fundamental studies. In the process of commercialisation iron was used after reduction of mineral matter rich in magnetite. One special source yielded a good ammonia catalyst and soon it was realised that an artificial mix of the analytically determined components of this mineral under exclusion of impurities yielded a stable catalyst after an oxidative fusion process followed by reduction in synthesis gas mixture. This finding described 1910 is still the essence of today's catalyst manufacture and activation. The procedures and the recommendations to use synthesis gas as reducing agent, not to exceed the reduction temperatures above 900 K and to subject the oxide to a flash heating to 1100 K immediately prior to reduction (i.e. to produce nonstoichiometry within the oxide) were all described in a series of fundamental patents in 1910 to 1911 (DRP 247852, 259702, 256855). We note that this information was accessible to the researchers giving the scientific explanation of ammonia synthesis without being used by them in any traceable way.

It is most interesting to learn that Mittasch used a combination of „physical“ (pore size distribution, bulk density, particle size) parameters which he was unable to quantitatively determine and „chemical“ parameters (promoters, nitride formation) which he could determine quantitatively as guidelines to the successful catalyst. The driving force for his development was the idea of a „metastable“ nitride as reaction intermediate and much in parallel to the ideas outlined in the Introduction he thought of the promoters as materials which support the formation or reaction of the central nitride species the previously determined stability of which led him to choose iron as the most successful catalyst candidate.

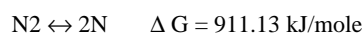
Ruthenium was first suggested in 1912 and patented as 5% Ru on MgO catalyst (DRP 292997,289105) operating at 80 bar and 723 K. It was noted that such catalysts should be specially resistant to poisoning effects. These promising experiments carried out by a research institute for the explosives industry were terminated after 1918 on grounds of cost arguments of ruthenium vs. iron. These studies are characterised by systematic research into metal-support interaction and described for Ru on chromium oxide systems effects which we would refer to as synergistic.

For a more detailed account on the history of the catalyst system see reviews of e.g. Topham [21] and Tamaru [22].

### 2.1.3. Thermodynamic aspects of the reactants

#### 2.1.3.1. Dinitrogen

The bond strength of dinitrogen is with 941 kJ/mole indicative of the stability of the triple bonded molecule with a short interatomic distance of 109.76 pm. The first ionisation energy is 1503 kJ/mole precluding a chemical way of direct oxidation. The Gibbs free energy for the dissociation reaction was determined to be



The data indicate that the comparatively cheapest method is the reductive activation with the formation of anionic intermediates which do, however, not exist as known chemical species.

#### 2.1.3.2. Relevant Nitrides

Most elements in the periodic table form one or several nitrides with several structural motives. For the present discussion the structure of interstitial compounds is relevant. In this structure family small main group atoms (or anions) are intercalated into voids (first choice octahedral) of the close-packed arrangement of the host metal structure. As the nitrogen atom with 70 pm hard sphere radius is larger than most interstitial sites in metals, only a small number of all available voids will be filled resulting in strained metal lattices. In cases where the nitrogen atoms do order tetragonal distortions result of the parent cubic elemental structures. In any case a wide range

of stoichiometries with poorly developed phase boundaries result from this structural principle [23].

The determination of thermodynamic data for dinitrogen activation is associated with the problem of ammonia synthesis as in both problems the cleavage of the strong N-N triple bond has to be achieved in a controlled way. This was realised already in early studies of the reduction of nitrides by hydrogen thought to be the mechanism of ammonia synthesis over iron [24]. For the formation of nitrides two solutions are used. In most cases the principle of virtual pressure is used and nitridation is easily accomplished with ammonia at elevated temperatures. Most thermodynamic data were obtained, however, with „activated“ surfaces. Deliberate introduction of defects by fresh evaporation, sputtering or suitable thermal treatments created surface defects which were reactive enough to dissociate nitrogen at around 300 K. The resulting heats of chemisorption [25] were found to be extremely dependent on „coverage“ which should be read as „saturation of defects by nitride formation“. The average value of  $200 \pm 20$  kJ/mole [7] was also found for single crystals from a kinetic analysis [26,27]. On technical catalysts the values scatter far more between 50 and 210 kJ/mole at various temperatures which is not surprising in the light of the difficulty to control degree of reduction of the oxide precursor.

The large variation in number and the strong dependence on coverage render it difficult to assign the data in the literature to an intrinsic chemisorption process. The most accurate gravimetric [28] determination on a controlled pre-activated catalyst gave values of

$-288 + 446.5 \Theta$  kJ/mole for low coverages (up to 0.22  $\Theta$ ) and

$-136 + 122.2 \Theta$  kJ/mole for high coverages

These data allow to conclude that the average value is representative for the initial heat of chemisorption. It is pointed out that under practical reaction conditions the value may be drastically lower if the chemisorbed atomic nitrogen is the *mar*i species.

The dissociative chemisorption of nitrogen on metallic surfaces leads to a state of adsorbed nitrogen atoms which is sometimes referred to as „nitride“ although they are dissimilar in their electronic structure to the nitride  $\text{N}^{3-}$  ion, which is found in bulk nitrides. The term „surface nitride“ was introduced to discriminate the unique location

and electronic structure of the chemisorbed species from those of bulk nitrides.

Much less data are available for Ru surfaces. A series of measurements on supported and K promoted polycrystalline samples revealed initial heats of chemisorptions between -90 and -150 kJ/mole [11].

The determination of thermodynamic data of ammonia chemisorption on polycrystalline surfaces is not possible without significant interference with nitride formation [29]. On single crystals thermal desorption data allowed to determine values of -71 kJ/mole for Fe (110) [30] and -84 kJ/mole for Fe (111) [31].

It is noted that the same trends and problems occur with the thermodynamics of the chemisorption of the catalyst poison oxygen. At low coverages the initial enthalpy of chemisorption of oxygen is up to 420 kJ/mole [32] dropping to less than 10% for full coverage. The reaction is fully irreversible and cannot be investigated with temperature programmed methods as dissolution and bulk oxide formation sets in.

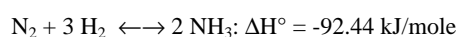
### 2.1.3.3 Hydrogen

The data for the enthalpy of chemisorption of hydrogen on single crystals as well as on technical catalysts and polycrystalline surfaces agree rather well in the span between -85 kJ/mole and -105 kJ/mole [33,26,34].

For Ru the chemisorption of hydrogen at low and intermediate temperatures is so strong that it poisons the ammonia synthesis. Above 431 K the inhibition is lifted and an extremely active catalyst results with a very difficult to measure kinetics (transport limitations). For the use of hydrogen to titrate the number of active sites on Ru see the literature [35,36]. It was found that the analogous procedure does not hold for iron catalysts as hydrogen is desorbed at too low temperatures to reside with appreciable coverages under reaction conditions on the active centres [37].

### 2.13.4. The reaction

The ammonia synthesis reaction is an exothermic reaction.



The precise thermodynamic data at reaction temperatures and pressures can be evaluated with extreme precision from the equation of state and the reaction equilibrium data. A recent review summarises the current most detailed data on these technologically most important quantities [38]. To be taken into account are the modifications of the phase equilibrium by mixing effects of the ideal synthesis gas with „inerts“. These gases are admixtures from the gas purification stages which do not poison the synthesis catalyst. Most prominent are argon and methane (technical mix: hydrogen, nitrogen, argon, methane 3: 1: 0.18: 0.44).

In Figure 2 the equilibrium conversion is shown for a stoichiometric gas feed. The drastic effects of both temperature and pressure are clearly seen. The beneficial high pressure effect is explained in all textbooks of physical chemistry as the principle of „Le Chatelier“ meaning that a change in molar volume shifts the equilibrium into the direction of a lower total molar volume. Figure 3 exemplifies the performance of technical catalyst operating at atmospheric pressure under steady state in stoichiometric feed at high purity (criterion: no delay in the output response to a temperature change). The characteristic shape arises from kinetic reaction control at low temperatures and from thermodynamic control at high temperatures (in Figure 3 above 710 K). The plateau is of mixed control type and allows under technical conditions the stable operation of the catalytic converter. The Figure shows that great care must be taken in the evaluation of the „activity“ of a catalyst without knowing the whole relation of conversion to temperature. Only at intermediate conversions and at low temperatures the quality of the catalyst expressed in an optimum of kinetically controlled conversion can be analysed. At high temperatures or at low conversions all catalysts are almost equal for either slow kinetic control or thermodynamically limited conversion. The difference in the two runs in Figure 3 is the temperature program of activation (24 h for run 77 and 50 h for run 98) of the same catalyst in the same reactor. The significant difference in performance calls for a detailed analysis of the process of catalyst activation.

In the discussion of potential advantages of biosynthesis of ammonia over the current technical process it is stressed that the high pressure process would be „inefficient“ and energy consumptive due to its „energy waste“ of compression and expansion [2]. To illustrate the efficiency of a modern ammonia plant the following points must be considered. Ammonia is required for further applications not as diluted aqueous solution but as pure gas at atmospheric pressure. It is thus not the conversion step alone but the total process efficiency which has to be considered. This includes the generation of the pure feedstock from the general equation:

0.4422 methane + 0.6155 water(l) + 0.6407 air  $\Rightarrow$   
ammonia (l) + 0.4424 carbon dioxide + 0.006 argon

(air: 0.2099oxygen, 0.7804 nitrogen, 0.0003  
carbon dioxide, 0.0094 argon)

At ideal efficiency, the energy which is required for one ton of ammonia irrespective of which synthesis strategy is chosen, equals the energy of ammonia relative to its decomposition into liquid water and air. This value is 4.73 Gcal/ton ammonia (gas, 300 K). Modern integrated ammonia plants can reach according to environmental conditions and technology values of 6.8 Gcal/ton or a thermodynamic efficiency of 70% for a technical product. This sets the limit for the discussion of the necessity to replace the current technology for reasons of energy efficiency. A full discussion of ammonia technology can be found in the recent literature [39].

### 2.1.3.5. Phase diagrams

For the analysis of structural aspects of the ammonia synthesis catalyst it is useful to refer to the relevant sections of the iron-nitrogen and iron-oxygen phase diagrams. These diagrams were determined in atmospheres of ammonia and oxygen, respectively, at a total pressure of 1 bar.

Figure 4 shows the iron-nitrogen phase diagram[40]. It can be seen that a  $\gamma$  phase co-exists with an  $\epsilon$  phase (phase boundary at ca. 8.25 wt% N). A phase boundary with pure iron occurs at 0.4 % nitrogen. Under the influence of nitrogen in the lattice the conversion temperature between  $\alpha$  and  $\gamma$  iron is lowered from 1170 to 870 K. This is of importance, as the solubility of nitrogen in  $\gamma$  iron is significantly larger than 0.4%. In the whole temperature window of ammonia synthesis down to 300 K the stable  $\gamma'$  phase exists with an average analytical composition of  $\text{Fe}_4\text{N}$ . The more concentrated  $\text{Fe}_2\text{N}$  phase is thermally less stable and occurs as linephase in the  $\zeta$  phase region. The  $\epsilon$  phase has an intermediate composition between  $\text{Fe}_2\text{N}$  and  $\text{Fe}_4\text{N}$  in the relevant section of the phase diagram.

In the light of this phase diagram and considering the concept of virtual nitrogen pressure [6] together with the thermodynamic results about the heat of formation for nitrides it is fully plausible that the surface of a working ammonia synthesis catalyst may exhibit the structure of the  $\text{Fe}_4\text{N}$  phase irrespective of the fact that this phase is thermodynamically metastable in nitrogen or inert

atmospheres at ambient pressure [6]. The fact that this nitride is an interstitial compound allows for a perfect epitactic relationship of the two structures as seen from Figure 5. In the (111) plane an almost perfect match of the lattice parameters exists with the nitrogen atoms located in octahedral voids causing a slight lattice expansion due to the oversize of the nitrogen atom. It is noted that the occupation of every possible nitrogen position will not be equal to one under synthesis conditions as the high activity of atomic hydrogen and the diffusivity of the nitrogen atoms in iron cause two antagonistic factors for reducing the steady state abundance of nitrogen atoms at the surface and provide the possibility to create a gradient of nitrogen concentration from the surface into the bulk of the iron. The formation of such situations with nonstoichiometric nitrides ( $\text{Fe}_{10-18}\text{N}$ ) and gradients from the surface to the bulk have been reported in a detailed study of the iron-atomic nitrogen system [23]. The lattice match of substoichiometric nitrides with elemental iron will be even better than for stoichiometric  $\text{Fe}_4\text{N}$  as a tendency to form chains of nitrogen-occupied octahedral sites will cause residual lattice strain only in the (110) direction of the interface.

This lattice epitaxy between the model iron surface and the iron species present under reaction conditions is one advantageous fact which contributed to the success of the single crystal work in mimicking quantitatively the catalytic process on the technical catalyst. In this special case there is no material gap between model and technical system caused by the high chemical potential of the reactants.

The discussion in the literature about a possible surface nitride [6] or a bulk phase with a segregation enthalpy for nitrogen of 107 kJ/mole [41] present in the active phase is not conclusive yet as all data have not been measured under ammonia pressures relevant for synthesis conditions. Instationary storage experiments probing atomic nitrogen [42] conclusively showed the presence of sub-surface nitrogen stored in the catalyst bulk. As the ammonia partial pressure of its generation was only less than  $10^{-4}$  of the value under technical conditions it can be assumed that a fair fraction of the activated iron will be present as nitride-type phase. The decomposition experiments in the literature [6,41,29] provide evidence for the most likely presence of  $\text{Fe}_4\text{N}$  structural units in an equilibrated system atomic nitrogen-iron metal.

The phase diagram for the iron-oxygen system is much more complex as seen from Figure 6. Only a section is displayed[43,44,45] containing the relevant phase boundaries which are crossed during synthesis and activation of the iron (dotted line).



The catalyst precursor is generated by fusion of iron oxides of various composition until a oxygen composition of ca. 52 at% is reached. This composition can either be obtained from thermal evolution of oxygen from hematite based oxide or by addition of iron-rich components to the precursor mix. At this point the promoters are added as oxides. Then a suitable cooling procedure is applied bringing some of the wuestite (FeO) as metastable solid into the regime of co-existing iron metal and magnetite[44,45]. The metastable phase mix of metal and several oxides is the essence of the catalyst precursor. Chemical reduction at temperatures below 830 K leads to the catalyst consisting of elemental iron and non-reducible oxides in small quantities. On this route no other phase boundaries are crossed meaning that mixtures of magnetite and iron metal are perfectly stable at any composition which in turn explains the kinetic difficulty to fully reduce the catalyst precursor. In the experimental literature the term „well reduced“ and „strongly reduced“ designates samples which are analytically free of magnetite. The phase range of syn-proportionation of Fe and FeO has to be avoided as in this range eventually also elemental iron is obtained but with a different internal texture than in the low temperature reduction process. The syn-proportionation destroys structural relationships between magnetite, wuestite and iron nuclei which are of extreme importance for the formation of ammonia iron [46,47]. The solubility of oxygen in iron in the temperature range of interest is with less than 0.01 at% very low.

The structural relationship between the iron-rich wuestite and the iron-poorer magnetite is illustrated in Figure 7. Both structures are dominated by their closed-packed arrangements of oxygen anions (large spheres). The close packing allows for perfect positional match as indicated by the arrows in Figure 7. The top structure of wuestite contains all iron in octahedral voids, whereas all tetrahedral positions are empty. The perspective view allows to see the octahedral co-ordination of the ferrous ions which are in the same arrangement as the sodium ions in sodium chloride. The lower structure in Figure 7 represents magnetite in a slightly different perspective to allow the view into the different void filling. Octahedral iron(light bonds) co-exists with tetrahedral iron (dark bonds) with both types of voids being incompletely filled. It can be seen that chemical reduction to wuestite can occur by moving the tetrahedral iron in every other layer into the partly empty octahedral void under expulsion of a rod of oxygen anions. It is obvious that the solid-solid state transformation associated with the chemical reduction can occur with a minimised movement of atoms but will be in its kinetics clearly topochemically controlled.

#### 2.1.4. Generation and Structure of the Iron Catalyst

##### 2.1.4.1 Some Reference experiments

The exact nature of catalytically active iron [46] referred to frequently as „ammonia iron“ was discussed controversially ever since the description of Mittasch [20] who knew that special requirements for its purity together with the necessity of the presence of synthesis gas during activation were mandatory to form a good catalyst. The correlation of these requirements with the catalytic function was unknown as well as the exact nature of the active phase. In this situation a series of reference catalysts was prepared and characterised chemically and kinetically in great detail by Boudart and co-workers [48,16,49]. The model system was iron particles supported on MgO. This system allowed a variety of techniques to be simultaneously applied, including Mössbauer spectroscopy, transmission electron microscopy, magnetic measurements, CO chemisorption and conversion experiments after different activation procedures. The iron metal particles were available in sizes from 1.5 to 30 nm allowing to study the variation in reactivity from mainly surface iron atoms to mainly bulk iron atoms. This range of particle sizes allowed further to apply the bulk-sensitive technique of Mössbauer spectroscopy to elucidate surface catalytic properties of the iron atoms. The MgO support was further of advantage as it could be shown that no metal-support interaction modified the properties of the iron particles with their varying size. In addition, it was shown that no promoters were present nor essential to allow for activity of these particles in ammonia synthesis which simplified the analysis of the mode of operation.

The first issue to check was the speculation [50] that ammonia synthesis is a structure sensitive reaction. This term meant that the *ton* should depend on the particle size as the relative fraction of different crystallographic faces changes with particle size [51]. The conversion experiments were further used to prove that atomic nitrogen reconstructed the iron particles into a form exhibiting a higher *ton*. This effect was described earlier in model experiments with iron tips in field emission microscopy studies [52,53]. The data revealed that iron reconstructed under the influence of atomic nitrogen into the (111) orientation. Using the principle of virtual pressure Boudart treated the iron particles with ammonia, thus providing a high virtual pressure of nitrogen. The most important results [16] from the catalyst testing are collected in Figure 8. The representation is special for ammonia synthesis as this reaction can be studied at equilibrium allowing to represent the conversion as efficiency. This quantity is defined as the ratio between observed ammonia production and equilibrium ammonia concentration under the conditions of pressure and composition used for testing. The *ton* contains the information about the number of active sites which was determined by CO chemisorption

[49]. The technical sample was a unsupported doubly promoted (alkali and structural promoters) iron catalyst. The data points indicate the results after activation in synthesis gas, the lines refer to activation in nitrogen-free hydrogen.

The data show first that ammonia synthesis is indeed a structure-sensitive reaction with a pronounced dependence of the *ton* on particle size. It appears that the often used rule „the smaller the catalyst particles, the more active they are“ is clearly not valid for ammonia synthesis. Well prepared iron metal particles are at least as efficient as the optimised technical catalyst under the conditions of atmospheric pressure and relatively low conversions which were chosen to detect kinetically controlled differences in activity and not transport limitations (see Figure 3).

- The data further show that ammonia activation is always superior to hydrogen reduction and that this effect is the more pronounced the smaller the particles are. By changing the sequence of exposures from ammonia to hydrogen and vice versa the authors could show that the effect is fully reversible. The time constant of the reversal was found to be large for small particles and smaller for large particles. In any case it was much larger than the estimated time for covering the iron surface with nitrogen atoms. From this and a number of other observations the authors concluded that a bulk structural modification occurs with exposure of iron particles to atomic nitrogen. This reconstruction was investigated in detail by Mössbauer spectroscopy and CO chemisorption measurements. From an accurate analysis of the qualitative and quantitative effects it was deduced that reconstruction creates preferentially (111) orientations on the surface thereby reducing the overall surface anisotropy which is characteristic for hydrogen-reduced particles. The Mössbauer data revealed further that sequential ammonia-hydrogen treatment reduced the recoil-free fraction of the metallic iron which was attributed to a decreased magnetic anisotropy of the particles. It could also be interpreted in terms of a decreased structural ordering of the iron, an argument which was not considered in the original discussion.

Figure 8 further exemplifies that ammonia synthesis is self-inhibiting as the *ton* decreases with increasing efficiency. It is pointed out that all these findings apply only to reaction conditions far away from the technical high pressure situation with efficiencies close to unity (plateau in Figure 3).

In summary, these data on a model system allow to conclude the following points for ammonia synthesis over iron which should also hold for technical catalysts:

- The reaction is structure sensitive with large particles being favourable for the *ton*. Irregular roughness or a maximum of surface-exposed iron atoms are not sufficient for effective ammonia synthesis.

- The promoter additives are helpful but not essential for the reaction which operates reproducibly and stable over well-prepared iron particles (contrary to findings with bulk iron which require promoters for sustained operation [54].)

- The active surface reconstructs under the influence of its own reaction product atomic nitrogen. The reconstruction is reversible by applying nitrogen-free hydrogen

- The reconstruction favours uniform surfaces with (111) orientation.

These statements are in agreement with earlier findings and ideas by Brill [53] concerning the nature of the active surface. These ideas are inconclusive, however, with respect to the mechanism of ammonia synthesis and the reason for the special relevance of the (111) orientation which was tentatively explained with molecular orbital arguments by several researchers [52,55] as indication for a dinitrogen molecular reaction intermediate. This *mar* would be bound effectively only on the (111) plane which exhibits the required trigonal symmetry of the iron d-orbitals.

In a recent series of experiments the course of the reduction of iron oxide particles ex iron cyanide salts supported on alumina and magnesia were studied as function of the water abundance and the nature of the support [56,57]. Using Mössbauer spectroscopy it was concluded that the reduction always produces wuestite ex magnetite as intermediate compound. At high water partial pressures the ferrous oxide phase is stabilised through an interaction with alumina or magnesia leading to a ternary oxide with the help of hydroxide species. At low water partial pressures a stabilisation of FeO only by alumina was also found but with a different mechanism not involving the formation of a ternary oxide. It was also noted that the onset of reduction occurred at lower temperatures if the water content of the precursor was lowered (by using different precursor chemicals). The same system was

studied by another group [58] with surface sensitive techniques and rather similar results were obtained regarding the ternary compound formation with alumina. The presence of an oxide or cyanide species as clearly seen by Mössbauer spectroscopy is rejected by the authors of [58] but their published XPS data are compatible with the presence of a divalent oxide species. Common to all this work is the identification of pronounced interactions of iron species with alumina which is promoted by the presence of water. Water seems further to support redistribution of the alkali salt component towards a coverage of the iron by potassium which was found to be beneficial for nitrogen absorption. It was further found [58] that the gas phase during activation had a drastic effect on the performance of the final system which was highly active after activation in synthesis gas. It was concluded that the iron-alumina interaction should be much weaker after activation in synthesis gas than after treatment with inertly diluted hydrogen.

The micromorphology of activated iron for ammonia synthesis was studied in series of experiments using iron-zirconium metallic glasses as model catalysts [59,60,61]. This precursor consists of a disk-like internal microstructure which can be preserved during crystallisation leading to aggregates of iron platelets separated by zirconium oxide spacers. This microstructure is long-term stable and exhibits a high *ton* relative to the data in Figure 8 allowing to conclude that on the iron disks the density of active sites is high due to its special morphology. Thermal treatment to isotropic iron without platelets creates an inactive catalyst with the same chemical composition. In this work anomalies of the X-ray diffraction pattern caused by ordered stacking faults and other disorder effects were observed. Again structural disorder seems to be an element of an active ammonia synthesis catalyst. These model studies created the idea [54] that an active catalyst should co-exist of stacks of platelets possibly exposing the (111) face as basal plane.

#### 2.1.4.2. The structure of the iron oxide precursor

Figure 9 displays a well-resolved powder X-ray diffraction pattern (XRPD) indicating all components constituting a technical catalyst for ammonia synthesis [62]. The main reflections can be assigned to magnetite ( $\text{Fe}_3\text{O}_4$ ) and wuestite ( $\text{FeO}$ ). Additional faint reflections are observed arising from calcium ferrite ( $\text{CaFe}_2\text{O}_7$ ), potassium hydrogen carbonate ( $\text{KHCO}_3$ ), and  $\alpha$ -iron (denoted as C, K, and  $\alpha$ -Fe in Figure 9). The pre-history of this catalyst precursor is reflected in the coexistence of magnetite, wuestite, and  $\alpha$ -iron within a single sample. This combination of phases is unique for the catalyst precursor as within one solid metastable phases both with respect to their oxygen fugacity and the phase equilibrium at ambient conditions

(see Figure 6) [54] do co-exist. Under topochemical control of the activation process a non-uniform agglomerate of elemental iron will be formed which in itself may be one explanation of the nature of "ammonia iron" [42].

Energy dispersive X-ray elemental analysis (EDX) in the electron microscope showed that the precursor material also contains some titanium, silicon and aluminium in addition to calcium, potassium, and iron. While some of the wuestite and the titanium and silicon components are not detectable by phase analysis with XRPD because of their X-ray amorphous microstructure, the presence of aluminium is indicated by distinct textural changes of the reflection intensities of the magnetite precursor. The fine structure of some reflections, together with a reduction of the lattice constant of magnetite point to the presence of a solid solution of magnetite with hercynite ( $\text{FeAl}_2\text{O}_4$ ) and additional calcium ions [20,22,23].

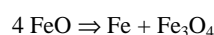
The example of Figure 9 is only one variety of structural modifications of the precursor oxide mix. Other examples have been treated in the literature [63,54,64,65]. Common to all materials is the significant structural deviation of ammonia magnetite from conventional magnetite caused by solid solutions with promoter oxides and a textural inhomogeneity with magnetite crystals separated by a grain structure filled with non-iron oxides and a glassy phase as detected by transmission electron microscopy and electron probe microanalysis[46,54,66].

#### 2.1.4.3. The activation process

All research in ammonia synthesis catalysts always emphasised the relevance of the activation step for the performance and stability of the catalysts. Technical catalysts are supplied with detailed prescriptions for the users for the activation process requiring control of temperature, time and water effluent partial pressure. The prescriptions either apply a slow linear heating ramp from 300 K to about 800 K over 100 h or use a two-step reduction with an isothermal break of several hours at the point of maximum water evolution (at ca. 650 K) with a much reduced overall activation time of about 40 h.[54]. Rapid activation within several hours leads to irreversible structural damage of the catalyst system [67] and poor catalytic performance (see Figure 3). The reason for this lengthy activation procedure lies in the reduction kinetics of the fused oxide precursor which comprises several well discernible steps becoming detectable in non-isothermal experiments only at heating rates below  $10 \text{ Ks}^{-1}$  [54].

Temperature-programmed reduction experiments of a technical catalyst (Haldor Topsoe KM1) in synthesis

gas are displayed in Figure 10. The DTG curves show some structure at low heating rates with the prominent pre-peak being due to the thermal decomposition of wuestite. This structure occurs also in inert atmosphere with significantly lower intensity indicating that the decomposition is assisted by the chemical reduction of the secondary magnetite arising from the dis-proportionation of FeO:



The main reaction occurs in several poorly resolved steps. This stepped reaction progress is not in agreement with a simple core-and-shell model of reduction as proposed from time-resolved studies [68]. The top panel of Figure 10 shows the conversion vs. temperature of the catalyst for two heating rates. Both TG curves lead to the same incomplete reduction degree of 90 % relative to pure magnetite (weight loss 27.7 %). The difference is due in part to the presence of the binary promoter oxide phases which reduce the abundance of iron oxides and convert during activation into ternary oxides non-reducible at the temperatures employed. It is noted that also in isothermal experiments an incomplete reduction was observed [69]. The formation of ternary iron containing promoter oxides which will not reduce at the low temperatures used here is also not excluded from these observations.

The DTA curve indicates by the feature above 960 K (line) that after reduction a further process occurs which reduces the sample weight only slightly but clearly modifies the heat capacity of the activation product. This process is very slow and can occur below 800 K at isothermal heating. All kinetic curves in the literature exhibit a slow final stage at reduction degrees above 80% which is not due to inadequate gas flow or particle size as carefully determined by Baranski and co-workers [69]. The effect indicates a post-reduction process which may be related to the development of the final porosity and the activity of the catalyst which also occurs only after completion of the reduction process [42].

It is noted that in a macroscopic experiment involving 150 g of technical catalyst it was found that even after 410 h reduction time at 850 K the catalyst still lost continuously some weight. The magnitude of the weight loss was found to depend on the initial temperature program and affected the ability of the catalyst to chemisorb nitrogen in a rather drastic way. This observation supports the view that the final structuring of the catalyst is a very slow process and may be understood in terms of a replacement of dissolved oxygen by dissolved nitrogen. An iron suboxide phase is replaced by a iron nitride phase which is beneficial for the nitrogen

chemisorption ability of the material.. The formation of the nitride may account for the pronounced effect of the slow process on the DTA signal in Figure10 which indicates a substantial heat of reaction to be associated with the slow final activation process.

The reduction of magnetite with hydrogen as part of the reduction of hematite to iron was studied also outside of the context of ammonia catalysts [70] and it was found that the reaction rate was positively affected by the presence of potassium whereas the presence of alumina had the adverse effect. These studies have shown that the topochemical reaction control is only operative in a certain window of reaction parameters given by temperature and reductive chemical potential. The kinetics can either be controlled by the reduction rate (chemical control) or by the gas diffusion through the product layer (diffusion control). Transition regions of a mixed control type were observed when the crystallites started to fracture into radially arranged fragments (pie texture). Most remarkable is the extreme case of reduction at high temperature and very high chemical reduction potential which is applicable to the case of ammonia catalyst activation. For the case of hematite to magnetite reduction the transformation of isotropic starting crystals into a lamella metastable form was observed by TEM images. This morphology is the consequence of conditions which favour efficient iron ion solid-solid interface diffusion without the possibility of a fast gas-solid interface reduction. Such conditions occur with a perforated skin of reaction inhibitor (iron metal, iron aluminates, alumina) at the surface of each grain and a high chemical potential for iron reduction around the holes of the inhibiting skin.

The scenario sketched in Figure 11 is so relevant for ammonia synthesis as it can explain how isotropic precursor crystals transform under the decisive influence of wuestite and alumina promoters into a unique metastable platelet morphology. If it can be shown that the activation process creates the (111) orientation as basal planes of the platelets, then it becomes possible to understand on a fundamental basis the successful modelling of industrial ammonia synthesis by the single crystal approach with macroscopic (111) iron single crystals. This point will be discussed later in this section.

Isothermal kinetic studies of the activation of technical catalysts as well as of partly promoted fused model oxides were conducted in great detail by the group of Baranski and co-workers [69]. The state of the art is reported in reference [68], a discussion of the severe slowing down of the kinetics by alumina and excess water is given elsewhere [71, 72]. The group uses a microbalance set-up with a very precise control of the gaseous

atmosphere in which the reduction takes place. In addition, the external particle shape and the chemical composition including the wuestite content are known for the catalysts specimen. In this way precise conversion vs. time curves for various materials (industrial catalysts and model systems with varying promoter contents) in several atmospheres („dry“ with about 100 ppm water and „wet“ with about 5000 ppm water) were established and analysed numerically according to a phenomenological kinetic model. This model has to take into account the following aspects:

- Wuestite reduces with a different rate law than magnetite [73], with the difference being dependent on the non-stoichiometry of the wuestite [74, 75]. In addition, the activation energies for the reduction of wuestite and magnetite differ significantly, as can be seen e.g. from Figure 10. The issue is further complicated as the iron formed by the wuestite decomposition acts as nucleation centre for magnetite reduction (Figure 11) [76] and exerts an autocatalytic effect on the magnetite reduction.

- The alumina promoter affect the reduction kinetics of magnetite, but not that of the wuestite. The mode of interaction proceeds via the water content which has no intrinsic effect on the kinetics of pure magnetite reduction.

- The potassium content exerts a reverse effect, i.e. it accelerates the reduction most remarkably in the presence of alumina. The acceleration effect does not depend on the water content of the atmosphere.

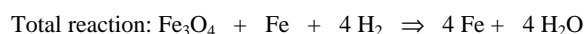
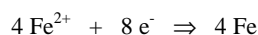
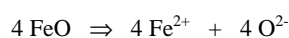
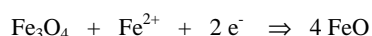
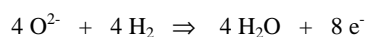
- As gas-solid interface reaction the transport properties of the solid for gases are of eminent importance. On the macroscopic scale this leads to a correlation of porosity with reduction kinetics [54]. On the atomic scale the volume reduction factor for the magnetite to iron reduction is the smallest of all iron oxides and the dense product layer iron metal will quickly inhibit efficient gas exchange at the reaction front.

The mathematical model used for the kinetic analysis [69, 68] assumes a particle of constant dimensions which converts into a porous iron shell and a non-porous initial magnetite core. The reaction front migrates in a topotactic fashion through the particle and conversion occurs only at the interface. The chemical reduction is assumed as a first order process. The reaction control is complicated by the diffusion of hydrogen and water through the porous iron shell. The model was successfully tested with pure magnetite [77].

In the light of the experimental facts described above, this model [78] contains many simplifications and is chemically questionable as molecular water diffusing through porous iron would immediately re-oxidise it. It is not too surprising that one of the three fit parameter of the model, the activation energy for the diffusion of water out of the shell yielded a value of about 130 kJ/mole which led the authors of reference [68] to the conclusion that the model is physically unfounded and remains despite its explicit physical assumptions a formal description rather than a mechanistic approximation. This is underlined by the fact that in wet atmospheres a simple parabolic rate law fits the data significantly better than the above described model. Finally, it should be mentioned that several other models were also developed to describe the reduction kinetics which, however, all fail to describe the experimental data. In view of the above cited complexity of the chemical reality it is not surprising that the simplifying models cannot describe the observations.

This is rather unfortunate as a valid description of the activation process could give insight into the structure of the active phase. The core and shell model would describe the activated catalyst as a porous derivative of the initial precursor mosaic crystals. A structural relationship would then exist between the precursor oxide and the active catalyst which would mean that the comparatively simple analysis of the oxide would allow to deduce a picture of the experimentally almost inaccessible active state of the catalyst structure. In practice, a wide spread in textural and compositional properties [54] of precursors lead after suitably adapted activation (main critical parameter is the water evolution kinetics in full agreement with the results of Baranski and co-workers [71,68]) to a comparatively homogeneous performance of the resulting catalyst, at least for the purposes of fundamental scientific considerations [47].

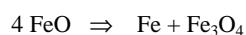
A more atomistic consideration of the reduction reaction reveals that the motions of electrons and reactions through intrinsic and extrinsic defects will determine the reduction kinetics. This was established in considerable detail during the study of the reduction of metallurgical magnetite [70,79,77]. A gradient in chemical potential of the iron ions is required for a suitable reaction progress. This gradient is built up by the iron metal nuclei which are essential for the process and which are supplied for the ammonia catalysts by the incorporation of metastable wuestite in the precursor mosaic crystals. Consequently, there will be no homogeneous topotactic reaction interface as assumed in the core and shell model. The active catalyst grows not as a shell around a precursor core but as a core within an oxidic matrix. The chemical equations [77, 42] for this model read as follows.



Kinetically this means that metallic iron is essential for the low-temperature hydrogen reduction of magnetite. In addition, the process is autocatalytic on a formal basis as the reaction product iron is in excess to the required educt iron. This behaviour can be coarsely found in the DTG trace at 1K/min in Figure 10. The effect is, however, much less drastic as expected from the net equation. The reason is the solid nature of educt and product. The educt iron (in fact two migrating electrons associated with a  $\text{Fe}^{2+}$  ion) has to be mobile whereas the product iron will crystallise onto the existing nuclei and will thus largely be inaccessible for initiating new reaction cycles.

All atoms of the final catalyst will have to move through the matrix. This will destroy the structural correlation between educt and product on an atomic scale. In addition, eventual restructuring processes are energetically simple as no high activation barriers for cooperative movements are required (see Figure 7). Further, the reaction rate will be heterogeneous in the mosaic crystal due to the distribution of extrema of the gradients of the iron chemical potential (distribution of the iron metal nuclei). Even within each crystallite of magnetite the reaction rate expressed as the mobility of the iron ions will be different for different crystal faces according to the centre density on these faces. For this reason a reproduction of the oxide crystal morphology in the final iron metal crystal is not to be expected in contradiction to the simple core and shell model.

In this picture it is the topochemistry of the iron nuclei which determines the shape of the grown iron crystals. It is most significant [70,80] that it is known that decomposition of wuestite proceeds by disproportionation into iron and platelets of secondary magnetite:



In this way a platelet microstructure (see Figure 11) of the resulting catalyst could be established which would not be present without any wuestite content. This could be one first hint towards the difference between ordinary iron and ammonia iron.

The activation kinetics was also investigated by state-selective in-situ Mössbauer spectroscopy [73]. A technical catalyst and synthesis gas were applied. The activation temperatures had to be chosen very low at 623 K to 723 K in order to accumulate sufficient Mössbauer absorption within each time interval. The spectral analysis yielded conversion data for wuestite and magnetite and formation data for iron metal simultaneously. The numerical results given in the reference are replotted in Figure 12. The top panel shows a simple exponential analysis as given in the paper. One key point was a decreasing activation energy with increasing conversion which seems in the light of the data set not fully supported. The other observation was a correlation of the reduction rate with the presence of wuestite in the way that the conversion of magnetite was faster as long as it was co-existing with wuestite. This observation is also questionable in the light of the errors in the data points as it is illustrated in the central panel of Figure 12. The data can be converted in relative reaction rates as illustrated in the lower panel of Figure 12. From these data it is clear that the reaction drastically accelerates after the wuestite is converted indicating that wuestite reduction is an independent process from magnetite reduction and that wuestite pre-reduction is beneficial for the magnetite reduction. Both points are compatible with the TG data of Figure 10 and support the view that wuestite reduction forms nuclei for the magnetite reduction which is an intrinsically much faster process than the wuestite conversion. It is not possible to decide if the turnover of magnetite is faster or if the number of reaction sites has increased by e.g. the opening of additional gas-solid interfaces from cracking of the magnetite-wuestite crystallites. The fact that the increase in rate between wuestite and magnetite reaction is smaller at higher temperature indicates the importance of kinetic reaction control for a topotactic reaction. At higher temperatures the reaction is dominated by a fast chemical reduction without allowing ion diffusion processes to control the topochemistry of the process. This is again in line with the sensitivity of the TG data in Figure 10 and in the literature [54]. Finally we see that after about two third of total reduction the rate is accelerated again which is also in agreement with the DTG data in Figure 10.

The role of the alumina promoter as rate-determining factor for the activation kinetics can also be rationalized in this model. As there is no gradient for the aluminium cations and they cannot be reduced to metallic

aluminium the oxide particles will not take place in the rearrangement of the iron matrix. They will segregate from the initial solid solution with magnetite[81] and form a kind of „ash“ in the reaction mosaic crystal. As its abundance increases at the end of the reduction process the ash will inhibit the iron motion or even encapsulate residual oxide patches(formation of iron aluminate, hercynite during activation). This could explain the general trend of a slow final stage of overall reduction. As the effect will be operational on each crystallite of the mosaic precursor crystal it may also act as a general retarding factor as observed in the work of Baranski. Early chemical analysis of the surface composition of activated iron catalysts revealed the idea of perforated skin of alumina covering the iron surface[82,83,64]. As the effect will occur at the surface of each crystallite in the mosaic crystal any final iron particle will contain a significant amount of alumina in its grain boundary region where it was located with X-ray diffraction [64] and Mössbauer effect measurements [84]. The ability of the alumina to spread over the final iron crystallite surface will depend on its own size. Larger particles will not cover the iron but remain immobile within the initial oxide matrix. In this way they will be incorporated in the growing iron particle and account for the small abundance of structural promoter affecting the Mössbauer data [84].

The observation of Baranski about the accelerating effect of potassium fits also in this picture as the alumina in highly alkaline environment will dissolve into aluminate  $[\text{AlO}_4]$  molecular complexes and so become more mobile. The fact that no potassium aluminate species can be detected by X-ray diffraction [67] which was used by Baranski to exclude this mode of action of alkali can be understood taking into account that aluminate is amphoteric and will precipitate out as alumina as soon as the alkali component is reduced in its local abundance. The participation of these effects is connected with the local concentration of molecular water acting as solvent (wet atmosphere) or as transport lubricant (dry atmosphere).

In summary, the presence of the promoters exerts a complicated influence on the reduction kinetics. As ion transport is a dominating process in the reduction mechanism it is to be expected that concentration gradients of the promoter phases will occur with the tendency to concentrate in the outer part of the iron crystal which grows from a nucleus to the outside and not from an external surface into the oxide particle, a reaction which would leave the promoters dispersed as they are in the precursor oxide.

The careful kinetic analysis of the catalyst activation and the failure to analyse these data in terms of

conventional gas-solid reaction models leads to the formulation of a more complex scenario which is schematically depicted in Figure 11. The central point is the incorporation of a iron cation motion along a gradient of  $\text{Fe}^{2+}$  ions created by the decomposition of an intermediate form of wuestite which forms the reaction interface. The term „wuestite“ does not designate large crystals suitable for X-ray diffraction but designates a zone of reactivity consisting of only  $\text{Fe}^{2+}$  ions in the oxygen lattice (see Figure 7) which is located next to an iron metal nucleus or particle. Such a concept will also be valid for the reduction of any normal iron oxide and could not account for the hypothetical special nature of the ammonia iron. The action of the promoters with their interference into the kinetics will lead under suitable external conditions of water partial pressure and temperature to a maximised anisotropy of the reaction rate. Most importantly, their presence will prevent the initially formed iron morphology to grow into the thermodynamically favoured form of large iron particles, a process known as Ostwald ripening or „sintering“. The freezing of the intermediate microstructure under operation conditions of the activated catalyst makes the difference to normal iron metal. This conjecture assigns to the promoters an additional function which not only creates the kinetic control of the activation but also preserves the product of the activation in the sense of the concept of structural promotion.

The activated catalysts is considered as a heterogeneous iron metal particle.. Around a core of perfectly normal bulk iron a metastable intermediate of the reduction process is arranged which is kinetically hindered by the presence of non-reducible spacer impurities to undergo structural transformations into the bulk iron stable form. Thermal activation and/or re-oxidation followed by re-reduction will allow to spatially rearrange the promoter impurities and the remaining iron which grows into one stable phase with the promoter ash spatially well-separated from it. The phenomena of transient ammonia activity upon oxygen poisoning as well as the irreversible thermal degradation effect of oxidised activated catalysts [85, 42, 46] would be compatible with it.

#### 2.1.4.4. Microtexture of the activated catalyst

The evolution of the geometric surface area of the catalyst is of importance for both the activation kinetics and the performance in ammonia synthesis as both processes are gas-solid interface reactions. A typical oxide precursor exhibits a surface area of about  $0.5 \text{ m}^2\text{g}^{-1}$ . After full activation surface areas of about  $18 \text{ m}^2\text{g}^{-1}$  to  $22 \text{ m}^2\text{g}^{-1}$  are characteristic [54, 42, 86]. The final surface area was found to depend for one particular oxide precursor sensitively on its pre-history with pre-oxidation or pre-reduction in pure

hydrogen before activation in synthesis gas reduced the surface area by 15% and 30% [42]. The value of the activated catalyst surface scales roughly with the geometric surface area of 30 to 50 nm large particles yielding  $15.5 \text{ m}^2\text{g}^{-1}$  to  $25.8 \text{ m}^2\text{g}^{-1}$  for cubic or spherical particles. This estimate indicates that the internal texture of the activated catalyst must allow access of the nitrogen probe molecule of the BET experiment to almost all of its internal surface. A mercury porosimetry study of carefully activated catalysts revealed a bimodal distribution with maxima at about 10 and 33 nm. The large pores develop at low reduction degrees, whereas the small pores occur first after 20% degree of reduction and account for all of the further increase in geometric surface area [87,63].

The evolution of the surface area in interrupted instationary activation experiments [54] is shown in Figure 13 together with the weight loss data for the same catalyst. In these experiments the surface area develops in parallel with the conversion as it was found in an early activation study [86]. It appears that a small increase in surface area is connected with the reaction of the wuestite which is necessary to start the main increase after the magnetite reduction is initiated. This observation is in line with the formation of iron nuclei and voids (of 33 nm average size) at the beginning of the reaction and the increase in porosity as the oxide is consumed. Such a behaviour is typical for a parallel reaction at many interfaces with little topotactic anisotropy.

If the activation is carried out isothermally at a low temperature such that 33 hours were required to generate all water (similar to a technical activation) then a quite different evolution of the surface area is observed as displayed in Figure 13 bottom trace [42]. The initial trend is similar as described above with the main difference that about 60% of the total surface area evolve from the last 5% of reduction, i.e. after the reduction of the bulk of the oxide. The conversion was with 96% very high in this activation experiment and the jump in surface area occurred in the region of the slow weight change described in Figure 10. The process indicates that the outer regions of the iron particles remain oxidised until the water partial pressure is very low due to the removal of most of the oxide. A particular high reactivity of the crystallite surfaces can be expected which may be beneficial for the ammonia synthesis activity. In the final period of reduction a structural rearrangement of the crystallites seems to take place such as to allow the formation of the smaller pores detected in the porosimetry study. At this point the promoters have to prevent the reaction of the active iron faces of adjacent iron particles to form larger isotropic bulk iron crystals. Under the non-isothermal conditions of the experiment in Figure 13 (top) the final surface area remained 20% smaller than in the isothermal experiment.

This and the different temporal evolution indicate that the microstructure of rapidly activated catalysts and slowly activated ones may be different. The creation of the textured structure of each iron crystallite can fully develop only under slow activation conditions. Sufficient time then is available for the complicated migration of the iron ions according to the reduction gradients and the functioning of the promoters as agents inducing the textured structure by their exsolution profiles. Rapid activation creates too many nuclei and causes isotropic crystal growth with no temporal separation of the individual processes as can be seen from the diffuse reduction profile in Figure 10.

The surface texture of the activated catalysts has been studied with scanning electron microscopy [54, 47]. These data reveal that the activated catalyst surface after passivation consist of flat patches with micron sized crystals of exsolved promoter phases namely calcium ferrite and hercynite. At high magnification regular crystal edges in the 20-100 nm size range were detected. Rapid passivation creates a crack system [47] from the overheating of the crystallites during oxidation. These cracks decorate a platelet anisotropy with pronounced cleavage preferences in one direction.

Metallographic preparation of activated catalyst particles were already used earlier to reveal the texture of the material [46]. In a recent study [88] this technique was applied with electropolishing of the mechanically ground surface. The result of optical polarised light microscopy is summarised in Figure 14. The grain boundary structure is clearly decorated by a porous non-iron material. The structural promoter oxides forming the glassy phase or the oxide particles on fracture surfaces investigated by SEM (see above) fill the voids and create the family of large pores in the pore size distribution curve [63,86]. This can be seen from the linescan in Figure 14 taken along a grain boundary filled with the granular material revealing holes in the micron size range. The metal particles exhibit regular crystal faces but are by far too large to represent single crystalline particles as can be deduced from linebroadening measurements of X-ray diffraction data revealing a crystallite size of 30 - 80 nm [54,64,89,81,90]. The polycrystalline nature of the metal particles is also in line with the frequent inclusions of oxide scales seen as black holes in Figure 14. The light halos around each iron particle arises from partial oxidation caused in the passivation process of the activated catalyst. The fact that a well-developed boundary of equal thickness exists for the oxidised zone indicates the success of the careful passivation which had not destroyed the microtexture by uncontrolled local oxidation and simultaneous overheating.



The assignment of the granular material to promoter oxides and its distribution not only in the grain boundaries but also in the iron crystals was established by EDX point analyses of a prepared catalyst particle as displayed in Figure 15. The conductivity contrast image reveals the grain boundaries and the many small inclusions as insulating material. But also the conducting homogeneous areas consist not only of iron but small amounts of structural promoter oxides (point 3). The insulating areas consist of a varieties of mixtures of oxides as can be seen from the analyses of points 1,2,4 in the image. The electronic promoter potassium can be immobilised in silicates as seen at point 2.

High resolution SEM data of „homogeneous“ areas of the electropolished iron crystals showed a further level of structuring as can be seen from Figure 16. A „sponge“ structure with anisotropic objects and small oxide inclusions (dark) appears giving an impression of the gas transport channels in the „solid“ activated catalyst. Linescans perpendicular and parallel to the grain boundary (straight line in the lower right of Figure 16) reveals the anisotropy of the particles by the anisotropy of the roughness. The texture is built from stacks of objects of below 100 nm individual size which can be assigned to the individual crystallites seen in the x-ray diffraction experiments. The stacking anisotropy extending over large areas of the large crystals will account for intensity anomalies seen in the XRPD data.

#### 2.1.4.5. Microstructure of the activated catalyst

In this section the structural details on an atomic level of the activated catalyst will be discussed. This issue has created a great deal of controversy during the history of ammonia catalysis research as reports concluding that pure elemental iron[54,84] is the active catalyst were contrasted with studies in which the special nature of activated ammonia iron was related to a unique non-iron metal crystal structure with endotactic defects causing the crystallographic effect of paracrystallinity [90,81]. The presence of alumina inside the iron metal lattice was also established by determinations of the phase transition temperature between alpha and gamma iron which was found to be too high relative to pure iron. Progressive cycling through the phase transition lowered the value back to its normal value indicating a phase separation and stress-induced precipitation of the impurity [65]. It is pointed out that the phase transition temperature is above the recommended reaction temperature for iron catalysts and that alpha iron-alumina mixed systems are metastable in the temperature window of their activation.

Activated and used catalysts may consist not only of iron metal but may contain a skin of a metastable form of an interstitial nitride  $\text{Fe}_4\text{N}$ [6]. Also amorphous structures for the active iron form [54,67,60] were taken into consideration. These controversial findings indicate that a detailed structural study is difficult to perform and will require in-situ diffraction experiments which have been performed recently [62]. On the other hand the clarification of the structural nature of the activated catalyst is essential for a rational application of the single crystal model study approach, as the incorrect choice of the substrate evidently prevents any meaningful physical model of the reaction to be studied.

The presence of promoter species has not only a decisive influence on the formation of the active catalyst but also on the performance. The concept of structural promoters summarises the presence of non-reducible oxides such as alumina, hercynite or calcium ferrite as to prevent the sintering of the activated iron into low-surface area large crystals. This may be accomplished by the presence of either a particulate form dispersed between the iron crystals or in the form of a thin skin over the catalyst surface. Early chemisorption data [82] on a technical reference catalyst [91] which were supported by Auger analytical data [92] are in favour of such a microstructure as well as modern surface spectroscopic investigations on industrial catalysts carried out after in-situ activation [93,94,54]. Such a skin can explain why only a small fraction of the nitrogen BET surface area is found to be of iron metallic nature[82,95]. The polycrystalline model systems discussed above reveal that pure iron is a suitable catalyst for ammonia synthesis. The formation of an iron-nitrogen compound during operation seems also to be of significance in the model systems[96]. A microstructure consisting of a normal iron particle surrounded with a patchy layer of non-iron oxides is thus the alternative to the suggested modified bulk structure of ammonia iron.

A variety of techniques and experiments has been used to decide between these two models of the active phase. The essential results will be discussed followed by a detailed description of in-situ diffraction work yielding a microstructure model which accounts for all experimental observations.

Mössbauer spectroscopy is a bulk analytical technique which indicates sensitively the local chemical environment of iron atoms. Any modification of the average iron metal structure by endotactic impurities would affect sufficient iron atoms to cause absorption lineprofile modifications. Disperse iron-noniron ternary oxides would disclose themselves by quadruple split lines with  $\text{Fe}^{2+}$  isomer shifts. Amorphous species would occur as

components with low-recoil free cross sections and hence modulate the background of the spectrum.

A comprehensive and critical review of the work of three different groups on this problem is presented by Topsoe and co-workers [97]. In this review it was pointed out that only in-situ experiments are suitable for the microstructural evaluation as the ex-situ passivation products (see Figure 14) cause Mössbauer absorptions exactly of the kind as expected for the bulk-modified iron model. The in-situ experiments exhibit the disadvantage to be performed at high temperature at or above 300 K. This could reduce the recoil-free fraction of defective structural components below recognition. In addition, the analysis of the review shows that no in-situ experiment was ever performed on technical samples which were activated in synthesis gas. This is an interesting contrast to the accurate work on synthesis gas activated model catalysts described in section 2.1.4.1 [17, 98] which gave essential clues on the structure-sensitivity of ammonia synthesis.

The present conjecture [99,100] can be summarised as follows. About 95% of the bulk catalyst consists of pure alpha iron with absolutely no sign of a structural anomaly. The remaining iron occurs as trivalent and divalent oxidic species and is attributed to particles of non-reducible ternary oxides (hercynite, calcium ferrite). The size of these particles is at or above 10 nm. The presence of small particles of non-iron metal particles was carefully ruled out within the above mentioned limitations which did also not allow to detect the possible formation of nitride species.

The Mössbauer data rule out the endotactic model and the aluminium skin model and support a spacer particle or the „combined“ model sketched in Figure 4. It is further noted that the line profile of the alpha iron pattern gave no indication for substantial stress or strain in the reduced material as it was suggested in the interpretations of the X-ray diffraction data. The by far most iron atoms are under the condition of sample activation applied for these studies in *one* perfect local chemical environment.

This conclusion can be tested using EXAFS Fe K-edge data which allow to determine with an even higher precision the local iron environment without the requirement for a crystalline phase. This means that even if an amorphous promoter-induced special structure would exist within ammonia iron it should be detected in EXAFS. In a true in-situ activation study [99] it was found that several phases of iron oxide occur during reduction. In addition, the first iron metal particles were detected at 600 K far below the main reduction temperature. These results

strongly support the activation scenario described above. An additional promoter effect was found for potassium lowering the activation onset temperature by 40 K relative to a sample promoted with caesium. This is also in agreement with the above findings.

The activation was completed at 650 K to 690 K and yielded an EXAFS Fourier transform spectrum identical with that of alpha iron. No indication was found for the existence of a non-alpha iron phase nor for an unusual stress or strain environment (lineprofiles of the radial distribution function). An anomalous low intensity of the EXAFS amplitude was stated which would point to a lower co-ordination number as in bulk iron, an effect normally found in cluster compounds. A cluster nature of the activated iron was, however, excluded by absence of any evidence for this in X-ray diffraction and Mössbauer spectroscopy. It is noted here that in this study no technical catalyst but a model catalyst was used with unknown precursor structure and catalytic performance.

A sample of a technical catalyst was studied by ex-situ EXAFS [54] after activation and kinetic characterisation using a Be air-tight sample container and a well defined sample geometry prepared in a glove box. This complementary study to the in-situ work arrived at the same conclusion and stated again no sign of any special iron environment in the ammonia iron. The intrinsically better sample geometry allowed to raise the level of confidence for the comparison of the EXAFS data between iron powder and the catalyst by extending the range in k-space and by an improved signal-to noise ratio. The lack in intensity was also stated but to a much lower extent than in the in-situ study.

EXAFS data support the structural model derived from Mössbauer spectroscopy and rule out the significant abundance of iron atoms in unusual geometries. The method is bulk-sensitive and cannot detect the small fraction of surface iron atoms which must have, of course, irregular geometries. This sets a detection limit for the abundance of the irregular phase. Any effect detectable in X-ray diffraction should, however, have been detectable in EXAFS too. The possibility to assign a special average bulk structure to ammonia iron is ruled out according to these experiments.

X-ray diffraction is maybe the most sensitive tool for the detection of bulk structural anomalies due to the extensive possibilities of accurate data analysis [101]. This data analysis can give details about the average crystal structure, the mean shape of the crystallites within a mosaic crystal and even about micromechanical stress and strain

in the particles. For a reliable analysis the X-ray diffraction experiment requires external input such as the chemical composition and information about the local geometric environment such as presented above.

An early study [91] of the microstructure of the oxide and the activated catalyst stated already a drastic effect of the promoters on structure and on catalytic activity the correlation of which was attempted first. Aluminum oxide was found to be the most effective promoter in a series of fused catalyst from a commercial source. In this paper the existence of wuestite was detected first and the position of the main diffraction lines was reported. The magnetite matrix was found to be slightly affected (lattice contraction of 0.15% for 3% Al in iron oxide) by the incorporation of Al into the lattice giving rise to a spinel. The structure of hercynite was described first. In-situ reduction transformed the coarse oxide crystals into small iron particles of „colloidal particle size“ with significant line broadening of the diffraction pattern. No sign of any anomaly of the lattice parameter (285.9 pm) of the alpha iron was noted irrespective of the composition of the precursor oxide. The reduction in particles size and the corresponding increase in surface area was shown to arise from the alumina content which was thought to inhibit sintering. The concept of structural promotion was described. The hardness of the ammonia iron as compared to the ductility of pure iron was noted and traced back to the location of the alumina in spinel form in the grain boundaries acting as inhibitors for crystallite gliding. Finally it was found that ammonia iron is metastable and transforms above 900 K into low-surface area normal iron plus exsolved oxide. This process destroyed almost all catalytic activity. The report is the first account of a structural difference between ammonia iron and crystallographically pure iron.

The importance of alumina in the ammonia catalyst structure was further investigated in detail at BASF [63]. It was confirmed that alumina formed a spinel phase and is present in solid solution with the precursor oxide. After activation it was found to form small particles separating normal iron particles of 10 nm to 100 nm diameter. The amount of beneficial alumina was carefully optimised by correlating catalytic activity, BET and CO surface areas with the alumina content. The CO surface area titration revealed that pure iron exhibit the same iron metal surface area as its geometric surface area which was, however, with 1.6 m<sup>2</sup>/g very much lower than the geometric surface area of the optimum promoted catalyst with 22.5 m<sup>2</sup>/g. In this state only 45% of the geometric surface area were accessible for CO, a fraction which reduces to below 20% for higher alumina loading. It was estimated that at optimum loading the alumina could form a

monolayer film of spinell on the geometric surface area of the iron.

This report showed that alumina is vital for the creation of the high surface area in the same way as it is necessary for the conservation of the small particle size. This effect has to be seen in context with the strong inhibition of alumina on the reduction kinetics which allows the heterogeneous nucleation of the wuestite to remain the controlling factor for the particle size of the iron metal. The idea about the monolayer film shows that the spinell must be present in two forms (two-dimensional patches and three-dimensional particles) in order to allow for the presence of free iron. At the optimum loading of 3% Al a free surface area of 10m<sup>2</sup>/g of iron in a material with 22 m<sup>2</sup>/g geometric surface was available yielding a maximum activity. The correlation between iron surface area, activity and Al loading was replotted from data of reference [63] and is shown in Figure 17. At a first glance there is a correlation between activity and free iron surface area. From this figure it is clear why no correlation of activity with the BET surface area or the particle size of promoted catalysts can be expected. Al increases the total surface area up to about 2% addition but decreases the fraction of iron exposed with higher loading. The specific relative activity per unit iron surface area is reduced upon addition of Al to the oxide precursor. This implies that Al reduces almost independently of its abundance the number density of active centres on iron or interferes with the elementary steps of ammonia synthesis which would be incompatible with the idea of a structural promotion by aluminium.

This effect is not due to a modified accessibility of the iron surface by a modified pore system. It was found [63] that a bimodal pore size distribution is formed by the addition of Al with large pores (micron size) being present in all catalyst compositions, while small pores (ca 30 nm diameter) were formed as consequence of the addition of Al to the oxide with a maximum abundance of the small pores occurring at 3% Al addition. The enhancement of the BET surface area could be traced back exclusively to a reduction in particle size by comparison with TEM and X-ray diffraction linebroadening data. The formation of porous iron metal crystallites can be clearly ruled out. All structural promotion must take place in the grain boundary system of the iron formed. Keeping in mind that in the reduced catalyst the Al must be present in both particulate and film form it can be concluded that small additions of Al first form a patchy film between the iron crystals. Upon addition of up to 3% Al the increase in surface area adds to the effect of film formation and increases the porosity. Above the 3% limit an additional site blocking effect without compensation by an increased BET surface area blocks small pores and reduces the iron metal surface area.

The modified specific activity per iron surface area points to a microscopically inhomogeneous site distribution and to an inequality between sites for ammonia synthesis and CO chemisorption. Al seems to modify the ratio between CO chemisorbing sites and ammonia synthesising sites in an unfavourable way. The beneficial microtextural effects overcompensate this catalytically negative effect of aluminium on the molecular scale.

The effect of Al on the catalyst was further investigated by high precision X-ray diffraction techniques [81,90]. For the oxide system the co-existence of magnetite, wuestite and hercynite was verified, a result which was confirmed recently [54]. Precision lattice constant measurements revealed a value of 839.0 pm for magnetite and 813.5 pm for hercynite. The linear relationship between lattice constant and fractional abundance of hercynite in magnetite was found to end at 3% Al in magnetite. At this point the system spontaneously exsolved in three phases with varying Al content. This finding explains the „magic“ number of 3% in the activity vs. composition plot of Figure 17. At this level the atomic dispersion of alumina in magnetite leading after reduction to very finely divided oxide particles and the formation of the alumina film end and is replaced by the formation of large crystallites of ternary oxides which cannot reduce during activation conditions and remain this as ineffective, only site blocking particles in the activated catalyst.

A series of iron oxides [81] promoted with varying contents of alumina were reduced in flowing hydrogen at 673 K and passivated by traces of oxygen. A second temperature treatment up to 900 K revealed the metastable nature of the initially obtained product. After this treatment the samples were studied by high-precision X-ray powder diffraction. All samples showed only alpha iron as crystalline phase after complete reduction. The particles were reduced in size from over 150 nm in the oxide to 50 -25 nm in the metal with the increasing alumina content causing smaller particles. Wuestite and Mg contents were found not to affect these values. The lattice constant was found to be close to the expected value with, however, a systematic deviation to larger values with increasing Miller index of the reflection used. This phenomenon is known in powder diffraction as paracrystallinity and occurs in many partially disordered systems.

Mössbauer spectra revealed normal alpha iron with slightly broadened resonance lines and a trace amount of hercynite with a nominally higher Al content than in the oxide precursor. The oxide became enriched in the aluminium impurity during activation. The presence of alumina in chemical contact with iron on the surface of

activated (and passivated!) samples was substantiated by SIMS [102] measurements revealing a series of fragments which allowed to conclude that a ternary oxide and not a physical mixture was present.

The anomaly of the iron reflections was excluded to arise from dynamic disorder as high temperature treatments caused a change in the pattern only above 1200 K at which temperature a phase segregation into gamma iron and alumina was observed. In this way it was assured that an aluminium containing heterostructure should be responsible for the X-ray diffraction anomaly. All data were consistently interpreted by the model of endotactic intergrowth of hercynite molecules into the iron lattice. It was found that one hercynite molecule fits into the space required for seven iron metal atoms. A slight misfit of this „molecular epitaxy“ would cause an elastic distortion of the iron lattice planes which will give rise to the paracrystallinity in the diffraction pattern. This deformation was also thought to limit the particle size as the kinetics of crystal growth will be affected by the imperfection of the surface geometry caused by the statistical intergrowth of the hercynite molecules.

This model which assigned a special crystal structure on the atomic level to ammonia iron caused considerable controversy in the literature and raised the fundamental question about the relation of bulk crystal structures to surface catalytic activity.

The material from the paracrystallinity study [90,81] was reinvestigated by another group [84] with X-ray diffraction and precision Mössbauer spectroscopy. The presence of high-purity alpha iron was found. The stated line broadening of the Mössbauer absorptions were attributed to the presence of clusters of alumina of 3 nm size within the iron metal causing macroscopic strain. Very careful reduction procedures and measurements excluding contact with air allowed to exclude any endotactic oxide as postulated from X-ray diffraction.

The same group investigated later the industrial catalyst used in the early X-ray diffraction study [91] again with Mössbauer spectroscopy and X-ray diffraction. The data are presented within a review paper on microtexture [64]. The sample contained more alumina than the exsolution limit found by Hosemann [81]. It was reduced with pure hydrogen and yielded iron particles of 61 nm size. The diffraction pattern showed also paracrystallinity and the Mössbauer spectrum revealed 1% ferrous ions in the sample. These findings were then interpreted as support for the endotactic model: „ All data presented are compatible with Hosemann“. But it was also stated in the

same paper that a model with a patchy skin of alumina would be compatible with the data. The alumina content was divided into three locations namely 10% within the iron crystals (endotactic of clusters), 5% as patchy monolayer and 85% as extra phase within the intergrain space.

Using the hydroxyl groups present on alumina it was possible [103] by selective deuterium exchange to determine the abundance of alumina on reduced catalyst. The results showed a significant coverage of iron by alumina but it was stated that not all alumina present can be accounted for by the film. This experiment which was repeated several times is independent confirmation of the heterogeneous distribution of alumina in the active catalyst.

The existence of the paracrystallinity anomaly was further shown in another study [65] of the activation of a 2% alumina containing magnetite with hydrogen at 773 K. The resulting iron particles were found to be anisotropic in shape with the equilibrium face (h00) being the small face and (hk0) being the long direction. A texture in (hkl) cannot be shown by X-ray diffraction due to symmetry reasons. It was found that the anisotropy remained after recrystallization at 1223 K which caused, however a significant increase in particle diameter. Using X-ray diffraction and differential thermal analysis (DTA) it was found that the mechanism of recrystallization is associated with the structural phase transition bcc to fcc at 1131 K (and not at 1223 K as stated in the paper) which causes segregation of hercynite. The DTA experiments further show that the alumina kinetically delays the structural phase transition whereas no effect on the magnetic phase transition at 1039 K (Curie point) can be seen in the data published. This can be taken as strong indication against the endotactic model and the continuous lattice strain which should affect the magnetic phase transition. The modified structural phase transition is well compatible with hercynite particles in the grain boundary region (such as in cast iron with graphite) and does not require a molecular dispersion of the impurity. This is also the conclusion of the authors who support the oxide cluster model.

The considerable experimental effort on the microstructure did not reveal a clear picture of the active catalyst which is required for a meaningful model study. Common to all results seems the presence of both particular and film-like aluminium oxides. Common is also the statement of the causality between surface area evolution and alumina content in the solubility limit of magnetite. Neither wuestite nor potassium nor magnesium had any microtextural effect. Common is further the confirmation of paracrystallinity and the slight broadening in the Mössbauer resonance of alpha iron. The reviewer states

besides the controversial model situation the fact that no study was done under in-situ conditions. Only in the old studies [91,63] ex-situ correlation between structure and activity are given explicitly.

In this situation a new in-situ high resolution X-ray diffraction study was carried out with the aims to clarify the possible texture of the resulting iron particles for which several literature studies had given some indications. In addition, the paracrystallinity phenomenon had to be explained in a different new way and the question about the presence of a nitride phase which could not be addressed by the ex-situ literature studies should be answered. Instationary conversion experiments strongly suggest [47] the formation of such a nitride which was postulated much earlier [6] as surface phase to exist.

The line of a powder diffraction experiment for an ideal mosaic crystal with domains large in dimension relative to the coherence length of the radiation is a sharp scattered intensity with a profile determined by the diffraction instrument used. Under these conditions the scattering can be described using a structure factor with a well-defined set of coordinates for the scattering centres in the unit cell. If the material becomes less-well defined the profile of a diffracted line will deviate from its ideal position and shape. The following reasons may apply:

- External stress or strain may cause a deviation of the Bragg planes from their ideal positions. This strain can arise from chemical compound formation between the crystallites of an iron crystal e.g. by sintering or during rapid anisotropic chemical reduction.
- Small domains within the mosaic crystal are irregularly dispersed.
- Structural defects occur within each Bragg plane in statistical distribution.
- The domains within the crystal are anisotropic in their dimensions and non-statistically oriented within the crystal.
- Endotactic chemical impurities are present with a non-perfect structural match (e.g. mixed crystals like hercynite in iron).

- Endotactic impurities are non-statistically distributed (e.g. with gradient towards the interior of each domain).

- Chemical strain is applied by an interdomain compound linking the internal surfaces with strong chemical interactions. The growth of a ternary iron aluminum oxide between two iron crystallites would cause such a chemical strain.

Any of these effects or combinations of them will cause the coordinates of the scattering centres within the structure factor to become distributions over a variation in distance. This distribution will fold into the lineprofile of the ideal structure and will cause observable distortions. If several reasons of positional distributions occur simultaneously, then the resulting distribution pattern can be bimodal. Under conditions of high resolution a second diffraction maximum at increasing distance from the main peak with increasing scattering angle will result. Exactly this was observed by the group of Hosemann [81, 90]. The above mentioned list of explanations will all cause the phenomenon of paracrystallinity for which the endotactic model is only *one* possible reason. It was the choice of these authors to reject all other explanations and to give the impression that paracrystallinity and endotactic hercynite in activated iron are synonyms.

Figure 18 shows the ex-situ XRPD data of an activated catalyst used for 500 h at 750 K at atmospheric pressure exhibiting all characteristics typical for a paracrystalline material. The paracrystallinity factor  $g = 0,99\%$ , the evolution of line broadening and deviations of the  $d$ -value for higher indexed reflections (a result of asymmetric broadening) correspond to earlier observations (Hosemann et al.  $g = 0,73 - 1,16\%$  [81], Borghard and Boudart  $g = 0,57\%$  [64]). In synthesis gas atmosphere, the reflection profiles of the active iron phase differ from symmetric lines of  $\alpha$ -iron expected at the temperatures applied. A close inspection of the reflection profiles displayed in Figure 18 reveals that an asymmetric broadening causes the shift of the centre of gravity of the profile giving rise to the paracrystallinity parameters.

In the  $2\theta$ -region of the Fe(110) reflection the diffraction profile function is best defined by the square of a Lorentzian<sup>2</sup> ( $L^2$ ) function, as it was verified by analysing the (220) reflection of the Si-standard. The  $K_{\alpha 1}K_{\alpha 2}$ -splitting of the X-ray source was considered for the fitting procedure and leads to an unconstrained fit to the typical ratio of 2:1 ( $K_{\alpha 1}:K_{\alpha 2}$ ).

From Figure 19 it appears, however, that the  $L^2$ -function does not fit the (110) profile of the "ammonia iron", even when the  $K_{\alpha 1}K_{\alpha 2}$ -splitting is involved. We note the deviation of the asymmetric wings in the profile of the difference pattern ( $R = 10,33\%$ ). In Figure 19 b it is

illustrated that a minimum of three pairs of lines were required to reasonably fit the measured profile ( $R = 3,68\%$ ). In-situ chemical modifications of the catalyst and the response of the profile analysis and the fitted model gave consistent results which we take as independent proofs both for the validity of the model and the existence of a correlation between catalytic performance and the bulk structure.

The observed Fe(110) profile is a convolution of the normal bulk (110) reflection ( $d = 204$  pm, FWHM =  $0,13^\circ 2\theta$ ) and one diffuse reflection at the same position ( $d=204$  pm, intensity 10%(110), FWHM =  $0,64^\circ 2\theta$ ) with a third contribution at a higher  $d$ -value ( $d=204,3$  pm, FWHM =  $0,25^\circ 2\theta$ ). The diffuse reflection at the Fe(110) position arises from defective elemental iron, while the main contribution reflection results from normal iron bulk material. The fact that two well-resolved contributions to the total diffracted intensity of alpha iron exist which is not adequately described by one average peak profile, is proof for a structural inhomogeneity of the iron. Regions of good crystallinity must co-exist with parts of much more disordered iron.

The second additional reflection is attributed to a phase with dissolved nitrogen which enlarges the lattice constants comparable to the formation of an intercalate species. This was verified by changing the synthesis gas atmosphere at isothermal conditions. The material was activated as described above. At 750 K nitrogen was removed from the synthesis gas feed. In certain intervals nitrogen was again supplied and thereafter removed another time. While the FWHMs and  $d$ -values change hardly, the systematic variation of the intensities is remarkable. Figure 20 summarises these results which reveal the merit of in-situ observations allowing to test the relation between structural inhomogeneity and the chemical environment. Diffraction data were taken for 15 h at each data point of Figure 20 in either  $H_2$  or synthesis gas atmosphere (data marked with + in Figure 20). The overall diffracted intensity remains independent of the atmosphere, but the relative intensities of the three contributions change depending on the presence of nitrogen. Removal of nitrogen lowers the intensity of the 204,3 pm-reflection, and the 204 pm-reflections raise. If nitrogen is added, the same process happens vice versa. The formation of the nitride phase occurs rapidly on the time scale of this experiment. The effects caused by nitrogen removal takes more time, as the bulk-dissolved nitrogen is only slowly consumed by ammonia synthesis. The response of the system to nitrogen partial pressure changes detected with a bulk-sensitive technique is full in line with earlier kinetic observations by Schütze et al. [42] and allows to rationalise the data from the group of Waugh [85]. The nature of this nitride phase which occurs not only as surface species [104] but also as a bulk phase has been discussed before. It is a nonstoichiometric interstitial compound with a composition lower in nitrogen than the surface compound

as can be deduced from the distance of the (111) reflection from the main reflection[23]. The results suggest, however, that dissolved nitrogen is not only at the surface of the working catalyst but also in the bulk where it modifies slightly the iron lattice with unknown consequences for the electronic structure [105]. It is pointed out that this effect cannot be avoided as it is a consequence of the high virtual pressure of nitrogen (several bars of ammonia) under synthesis conditions which is very substantially higher than under conditions of all model experiments

#### 2.1.4.6 Summary: the nature of the iron catalyst

The findings can be summarised in a model in which an explanation is attempted for the experimental observations of Hosemann et al. The model takes into account the definitive exclusion of endotactic epitaxy as cause for the anomalies. In addition, it should explain, why "ammonia iron" is textured in the (111) orientation which is a metastable termination in a bcc crystal.

In Figure 21 a graphical representation of the microstructure is shown. At the right hand side the basic ingredients are shown, namely crystals of bulk isotropic well-crystalline alpha iron (normal iron) and stacks of platelets exposing the (111) face as basal plane. Under synthesis conditions the situation as shown in the left hand sketch of Figure 21 will result. The iron core will be surrounded by a layer of nitride with an assumed gradient into the bulk of the iron. The platelets will be fully nitrated. The situation of bulk iron as support for ammonia iron (the platelet stacks) is a speculation and has to await experimental confirmation. The total size of such a particle which needs not to be isotropic as assumed in the Figure is in our case about 80 nm and can be smaller down to 20 nm depending on the activation procedure [54]. It is noted that the x-ray diffraction experiment cannot show that all three forms of bcc iron found in the lineprofile analysis constitute one single kind of particles as assumed in Figure 21. Micromorphological data suggest [106] that several different species of isotropic and anisotropic iron can occur in ammonia iron. At present it is, however, not clear how the relative proportions of the various iron forms are related with the correct activation of the iron oxide and how the sensitivity of the activated iron to micromorphological changes during sample preparation interferes with the TEM analysis.

While topotactic reduction should lead to isotropic dense materials as it is observed for metallurgical magnetite test specimen [79], the active catalyst consists of firmly adhering iron with a defined pore system. The strong texture of the magnetite precursor which becomes even more pronounced during the activation process [62] offers special directions for the reaction to proceed. While most of the material is consumed along the more densely packed (311) plane (gradually decreasing intensity of the  $\text{Fe}_3\text{O}_4(311)$  reflection), the (511) plane seems to act as a substrate for the growth of the anisotropic iron platelets.

The changing anisotropy of the reacting magnetite crystals indicates that no uniform and isotropic reduction of the precursor occurs and therefore no isotropic iron particles are formed. It is known that under precisely controlled conditions such reaction modes as described above may occur in iron oxide materials; Ettabirou et al. [79] and Gleitzer [70] showed that there is a competition in growth rate between the surface reaction rate and the diffusion of point defects (interstitial iron atoms) along semi-coherent interfaces of different iron oxides like in our case between magnetite and secondary wuestite. Under conditions of bulk diffusion control (high temperature, high reduction potential, slow overall rate) the growth of lamellae of the product starting from preferential spots of the surface was observed. Gleitzer introduced a fundamental model for the reaction mechanism [70] which we expand to the formation of the textured iron particles of the ammonia catalyst: Figure 11 schematically summarises the proposed reactions, the principal mass transport paths, and transformations resulting in the formation of iron lamellae. The principle behind this unusual growth mode of lamellae is the minimisation of the interfacial energy in selected directions allowing structural accommodation (epitaxy seems difficult but several planes of wuestite fit moderately well to magnetite (511)) and providing glide planes for the iron ions. From Gleitzer's findings in [70] it can also be rationalised why it was impossible [68] to distinguish between the two morphological models (core-and-shell and lamellae growth) from kinetic features of their formations as both time laws are very similar. Only the combination of reduction potential, temperature and reaction rate (hindered by promoter addition) selects between core-and-shell mode and lamellae mode leading to normal iron or ammonia iron.

The simultaneous occurrence of isotropic and anisotropic iron (see Figure 21) is controlled by the complicating factor of the presence of dissolved aluminium which prevents only in exsolved regions the sintering of the initially anisotropic iron by the spacer function of the structural promoter. In the process of activation several processes occur simultaneously, one of which is the concentration of the heteroelements in the still not reduced oxide. Only after a critical concentration of aluminium in the oxide has been surpassed the chemical potential will be oversaturated enough for alumina to exsolute as separate phase. The exact value of this threshold which will depend again on the overall reduction kinetics will define the degree of conversion at which the structural promoter spaces will occur in the system. At all earlier conversion the initially anisotropic iron will sinter and form the bulk isotropic iron which was detected rightly as main component in all structure-sensitive analytical experiments.

Poisoning experiments with oxygen [62] show clearly that a correlation exists between bulk structural features (anisotropy, particle size) and surface catalytic properties. These experiments further justify the bulk structural observations as relevant for the catalytic

properties of the material. The investigation reveals that the catalytically relevant surface structure is controlled by the underlying bulk structure. This structure can be created in a unique way by a suitable solid state dynamics which is technically controlled by the sophisticated activation procedures.

The microstructural analysis of formation and active state of the industrial iron catalyst for ammonia synthesis has given a new explanation of the old finding about the powder diffraction anomalies. It has further found one reason for the success of the single crystal approach in explaining the mode of operation on a quantitative basis. The model compound Fe (111) saturated with atomic nitrogen is identical to the technical system. The non-equilibrium (under ambient conditions) microstructure arises from a combination of a uniquely metastable mixture of precursor oxides and an activation kinetics allowing the topotactic reaction dictated by the iron ion diffusion to control the microstructure of the activated product. The promoters play an essential role not only in stabilising the final structure but also in ascertaining a slow reaction progress in a highly reducing chemical environment. The technologically undesirable fact of a slow activation is the key to the understanding why the unusual microstructure is formed which is catalytically so efficient.

The hierarchy of structural elements in the catalyst which became evident in the preceding sections is summarised in Table 2. The characteristic dimensions give the order of magnitude and can deviate in practical samples significantly from the values given. The relation between the dimensions remains, however, constant. The term basic structural unit (BSU) designates for iron the aggregate of Figure 21 which is „single crystalline“ under the coarse assumption of a homogeneous X-ray diffraction lineprofile.

Table 2. Structural hierarchy of the activated catalyst

Size	10 mm	10 $\mu$ m	100 nm	10 nm
Class	1	2	3	4
Solid	catalyst grain	iron crystal	iron crystallite	oxide spacer
Microstructure	polycrystalline	polycrystalline	single crystalline	single crystalline
Organisation	2	3 + 4	BSU	BSU
Voids	Intergrain pores	large pores	small pores	—
Size	100 $\mu$ m	3mm	30 nm	—
Filling	empty	porous oxides	spacers	—

This assumption is made on grounds of the significant spread of the fit results for different catalyst samples which are difficult to validate on a physical basis at the presently limited number of observations. The term „organisation“ classifies the relationship of the building blocks of each hierarchy step.

## 2.1.5. The Single Crystal Approach to Ammonia Synthesis

The preceding chapters revealed that the active component in the technical catalyst is iron with a particular texture. In order to approach the goal of devising a reaction mechanism based on observation of elementary steps it is essential to perform model studies with well-defined iron metal single crystal surfaces. A comparison of the effects of several crystal orientations on the elementary steps will clarify the reason for the structure sensitivity of the overall reaction besides the experimental verification of the rate-determining step providing the basis for kinetic modelling studies. The two main tasks of explaining structure sensitivity and elementary step identification were approached in a long-standing and continuous effort by a number of research groups. These results are summarised in respective chapters of a monograph [4,107] in which also major contributions from other groups are reported.

### 2.1.5.1. Single Crystal structures

A fundamental advantage of single crystal studies is the detailed structural control of substrate and adsorbate. The three principal faces of alpha iron were studied by low energy electron diffraction with the main results summarised in Figure 22 and Table 3. Several adsorbate structures of hydrogen and one structure of chemisorbed atomic nitrogen have also been quantitatively analysed with surface crystallographic methods. The structures of the clean low-index surfaces and of two adsorbate phases are displayed in Figure 23. It is pointed out, however, that the chemisorbed molecular nitrogen and chemisorbed ammonia have not yet been studied by surface structural methods. This lack of information is indication for the difficulty to prepare these adsorbates in a form suitable for analysis [108] which points to the limited stability of these intermediate products in the whole process.



Table 3: Structural parameters of iron single crystal surfaces and related chemisorption-systems (All distances are given in pm).

Surface	100	110	111	N	H
coverage	bare	bare	bare	0.5	0.5
LEED pattern	1 x 1	1 x 1	1 x 1	c (2 x 2)	(2 x 1)
surface symmetry	p4m	cmm	p3m1	p4m	pm
relaxation layer 2	95.1 %	100.5 %	83.4 %	107.7 %	99.0 %
relaxation layer 3	104.9 %	100.0 %	90.7 %	100.0 %	100.0 %
relaxation layer 4/5	100.0 %	-	104.0 % 97.9 %	-	-
shell 1	246.8 /4	248.5 /3	235.4/1	175.1 /1	181.5 /1
shell 2	284.3 /1	249.4 /2	244.3/2	204.3 /1	246.5 /1
shell 3	286.6 /3	286.9 /1	279.4/2	254.4 /2	247.8 /1
shell 4	403.7 /3	287.7 /1	394.9/2	286.3 /3	248.0 /3
shell 5	405.3 /2	-	405.4/3	297.0 /1	284.3 /1

The neighbouring shells refer to an atom in the top iron layer. The integers indicate the number of atoms on each shell (may be incomplete due to surface termination). The data are taken from the NIST structural data base SDD.

Figure 22 reveals that the three most densely packed faces of bcc iron exhibit the atomic arrangement corresponding to termination of the bulk structure, i. e. without reconstruction. The side views show that the (100) and (110) faces are closed surfaces with limited roughness whereas the (111) face is an open surface with considerable regular surface atomic roughness. A particular feature of the zigzag termination is the exposure of highly coordinated iron sites at the bottom of each valley. These sites having 7 nearest iron neighbours were termed as C7 sites [16,49, 109]. These sites which are a regular ingredient of (111) faces were identified in model studies [53, 163,110,111] as particularly active in ammonia synthesis.

The structural details and hence the electronic interactions are affected in different ways by the termination of the bulk. The iron-iron distance in the top layers is different from the bulk value (taken as 100% reference in Table 3) and is also different on different surface planes. The (111) plane exhibit the largest variation in interatomic distances due to its open character. It is further of interest to compare the analysis of the nearest neighbours in the structures between each other and with the bulk interatomic distance of 250.0 pm. The (110) plane exhibit the smallest deviations from bulk values whereas the (111) surface is again in this respect significantly different from the bulk structure. Bond distance variations of up to -6% relative to the bulk value may be taken as safe indications for a significantly modified surface electronic structure relative to the bulk situation. The next-neighbour distance of the top layer atoms in the (111) structure is with 235.4 pm shorter than in the bulk whereas the neighbour distance for the C7 atom is with 248.3 pm close to the bulk value. The minimal difference to the bulk metal value indicates that the local electron density is at this site the largest for all types of surface atoms on iron which is in line with the highest coordination number.

The H/Fe(110) system forms a series of ordered structures at low temperatures. The top structure in Figure 23 represents the case of a half-covered surface which is characterised by alternate rows of hydrogen atoms sitting in the threefold hollow position. At full coverage each row running in (100) direction is covered. The hydrogen atom occupies thus a high co-ordination site without, having, however, a close contact to the substrate as can be seen from the side view in Figure 23. The bonding is not central over the threefold site as follows from the different Fe - H bond distances of 175 and 181 pm. All this and the fact that the sum of the atomic radii of the Fe - H interaction is with 162 pm significantly smaller than the observed values indicate a complicated covalent interaction reflecting the modifications of the surface electronic structure of iron in its interaction with the hydrogen 1 s states. The observation

that the distance of the top iron layer to the second layer increases by 7.2 % illustrates that the bonding involves a fractional charge transfer from the iron valence band into the hydrogen 1s states forming a „hydride“ species. The situation is similar as with other metal hydrogen systems [112] and has also been studied theoretically [113,114]. The well-defined and non-dense arrangement of the hydrogen atoms indicates that besides the dominating adsorbate-to-substrate interaction there must also exist interactions between the hydrogen atoms which were deduced from theoretical considerations [115] to be of the order of 5 kJ/mole hydrogen compared to the sorption energy of 109 kJ/mole [116]. This small difference in energy explains why the long-range order disappears above ca. 200 K. This means that at ammonia synthesis conditions the hydrogen atoms are not present in a regular array but are highly mobile on the surface, a conclusion which is in line with the experience from other metal-hydrogen systems [112]. The structure in Figure 23 has to be considered as the frozen configuration at low enough temperatures.

This is rather different for the iron-to-nitrogen interaction. The structure of Figure 23 bottom for N/Fe(100) persists up to fairly high temperatures (600 K) [27]. At maximum coverage of 0.5 the nitrogen atoms are located in fourfold hollow sites. The side view indicates that the atoms are situated beneath the neighbouring atoms and form rather a sub-surface species than an adsorbate. The small nitrogen atoms with 60 pm diameter fall into the hollow site and interact strongly with the second iron layer as well as with the surface layer. This is reflected by the short Fe-N distances of 175.1 pm to the second layer and of 204.3 pm to the top layer. This strong interaction increases the top layer expansion beyond the value of the bare iron surface. The nature of the nitrogen-to-iron bonding is anisotropic with a strong direction along the „molecular“ axis and a weaker interaction perpendicular to it. The sum of the atomic radii is 196 pm classifying the bonding together with the anisotropy as covalent. The top view of the Fe N system in Figure 23 exhibits many structural similarities to iron nitrides (see Figure 5). A section through the unit cell of Fe<sub>4</sub>N along the (002) plane exhibits the same atomic arrangement and similar interatomic distances as the surface compound described in Figure 23.

#### 2.4.5.2. Energetics of chemisorption of hydrogen and nitrogen

The interaction of molecular hydrogen with metal surfaces leads even at low temperatures to dissociation and chemisorption of hydrogen atoms [112]. On Fe (110) it was found that the process occurs directly without a molecular precursor of detectable residence time and energetics. The

overall activation barrier for the formation of atomic hydrogen was determined to be 3 kJ/mole [117]. The chemisorption energy for hydrogen was determined on polycrystalline films [25] and on single crystals. It was found that the value was strongly dependent on coverage which was traced back to both surface heterogeneities and the hydrogen-hydrogen interaction. Initial chemisorption energies of 109 kJ/mole, 100 kJ/mole and 88 kJ/mole for Fe (100), (110) and (111) were determined [116]. The chemisorbed hydrogen recombines and desorbs from iron below 500 K [116]. This would imply that under conditions of ammonia synthesis the desorption process is so efficient that the sorption equilibrium will determine the surface concentration of atomic hydrogen. This result was derived under the assumption that UHV data are compatible not only with the temperature of ammonia synthesis (about 700K) but also with the pressure (100 bar relative to 10<sup>-8</sup> mbar) and that no pressure-induced phase change occurs for the hydrogen-iron system. The covalent nature of the iron-hydrogen bond which was deduced from structural arguments is compatible with the chemisorption energy and the detection of a bonding state in the Fe-H valence band at about 5.5 eV below the Fermi edge [116]. Theoretical considerations [118] and the experimentally found small dipole moment [116] are further confirmation for a complex bonding interaction of atomic hydrogen with iron.

The interaction of nitrogen with iron is significantly more complex both in terms of the number of species involved and in the nature of the Fe-N interaction. Four states of nitrogen have to be considered. At low temperatures two molecular precursor states for dissociative chemisorption have been identified. At high temperatures the migration of atomic nitrogen under the surface forming a sub-surface nitride species and eventually a bulk nitride has to be considered. This may transform the surface from a bare iron into an iron nitride and hence affect all surface electronic and even geometric properties.

The most weakly held molecular species can be prepared by exposure of iron to dinitrogen at temperatures below 80 K. At 100 K a thermal desorption peak labelled gamma state is observed which occurs both at single crystal faces [119] and on polycrystalline iron foil [25]. The chemisorption energy was found to be independent of the surface structure and was determined as 24 kJ/mole on single crystals [120] and 21 kJ/mole on iron foil [25]. The sticking coefficient of molecular nitrogen into this state was found to be remarkably high with 0.5 [120] allowing detailed studies about its bonding mechanism using photoemission (XPS, UPS) and high resolution electron energy loss spectroscopy (HREELS). In XPS the gamma state is characterised by a complex spectrum of two broad lines at 405.9 eV and 401.2 eV for nitrogen 1s

photoemission [121]. These two lines were assigned to different species in earlier work [122] but could be traced back to the edge-on bonding geometry [123] causing a chemical inequivalence of the two nitrogen atoms in the molecules which affect the spectroscopic core hole relaxation mechanism and hence cause the two peaks as final state effect [121,119,123]. In HREELS a N-N stretching vibration of  $2100\text{ cm}^{-1}$  was found which is close to the value of the free molecule with  $2194\text{ cm}^{-1}$ . The chemical bonding between iron and nitrogen is so weak that even the molecular Rydberg states of the free molecules could be observed with X ray absorption spectroscopy [108].

If the iron (111) surface is exposed to molecular nitrogen at 100 K a different molecular chemisorption state designated as alpha state is observed desorbing at 150 K. Its formation is more difficult to see as the sticking coefficient is with  $10^{-2}$  much lower and its preparation requires a clean and in the bulk nitrogen-saturated iron substrate [124,27]. The chemisorption energy was found to be 31 kJ/mole, in XPS the nitrogen 1s line shifts drastically to a narrow emission at 399.0 eV and in HREELS a frequency shift of the N-N stretch vibration to  $1490\text{ cm}^{-1}$  was observed [121,125]. These spectroscopic observations point to the existence of a nitrogen molecule interacting with both atoms with the iron substrate. This side-on configuration is found in only few molecular analogues preferably with electropositive main group elements such as Li organyl compounds. Their N-N stretching vibrations of  $1600\text{ cm}^{-1}$  and N-N bond distances of 135 pm (significantly elongated compared to 109.8 pm in gaseous di-nitrogen) were described [126]. The iron nitrogen interaction lowers the bond-strength in the molecule and allows for a pi bonding interaction [2] with the iron d-states donating electrons in anti-binding molecular orbitals. Angular resolved UPS-data [127] and theoretical considerations [121] support the picture of a pi-acceptor bonding between iron and nitrogen requiring a strong inclination of the nitrogen molecular axis relative to the surface normal. In this geometry the molecule comes into an intimate contact to the electron-rich iron C7 sites which can donate the electrons for the bonding. This idea is of great importance as it provides the understanding of the mode of operation of the catalyst. The C7 sites of iron are capable of activating chemisorbed molecular nitrogen by lowering the nitrogen-nitrogen bond order when occupying the pi-acceptor states. The binding ensemble comprises several atoms and does not contain only the most exposed top surface atoms. The specific spatial requirements further can explain the observed structure sensitivity of ammonia synthesis which was found to operate best with particles exhibiting the (111) orientation [64,3,128,53]. It is interesting to note that theoretical considerations predict for molecular model complexes a reduced stability for the side-on complex than for the end-on complex due to the

smaller energetic effect of the pi-back-donation interaction compared to the sigma donation interaction requiring the end-on geometry [129]. This prediction is well in line with the experimental observations and with the notion about the role of an alkali promoter.

If the (111) surface covered with alpha nitrogen is warmed up, in parallel either desorption from the molecular state or dissociation takes place. The adsorbed nitrogen atoms thus formed may recombine and desorb as beta state around 800 K [26, 27]. In XPS a single line at 397 eV is observed [121] which is also characteristic of metal nitrides. The formation of this atomic species (no N-N stretching vibration in HREELS, single UPS N 2p line at 5 eV below the Fermi edge) is associated with drastic structural rearrangements of the iron substrate as seen by series of complex LEED patterns [26,385] which did not occur on Fe (100) even upon drastic exposure to nitrogen. On this latter surface the nitrogen atoms can directly be incorporated into the top atomic iron layer as discussed above. The complex rearrangements and the observation [25] that stepped surfaces restructure into complex facets point to a strong iron-atomic nitrogen interaction with a nitride bonding which transforms a given iron surface into the (111) geometry for an optimum spatial arrangement. The resulting surface structure is a section of the bulk  $\text{Fe}_4\text{N}$  structure which is stable under high virtual pressures of atomic nitrogen (compare the low sticking coefficient of beta nitrogen) and was termed as surface nitride [26, 130]. Using isotope labelling experiments it was shown [26,385] that the surface atomic nitrogen can exchange with a reservoir of bulk atomic nitrogen implying that sub-surface nitrogen species will also be present under stationary ammonia synthesis kinetics. This is of interest in the light of the long known observation that iron nitride is an inhibitor for ammonia decomposition [29].

Table 3 summarises some characteristic properties of the surface species of adsorbed nitrogen. The data are collected from the literature cited above and refer to the (111) plane as substrate without any promoter present. The table also includes some data on sorption kinetics which will be discussed below. For a better orientation the collection of data is given at this point.

Table 3: Some characteristic properties of adsorbed nitrogen species

Species	g nitrogen	a nitrogen	b nitrogen
bonding	molecular	molecular	atomic
geometry	end-on	side-on	reconstruction of substrate
N-N stretching vibration (cm <sup>-1</sup> )	2100	1390	450 *
saturation coverage	5.8 μmole/m <sup>2</sup>	1.16 mmole/m <sup>2</sup>	Fe <sub>4</sub> N type surface nitride
desorption temperature (K)	90	160	860
sticking coefficient	0.7	10 <sup>-2</sup>	10 <sup>-7</sup>

\* Fe-N vibration

### 2.15.3 Structure and energetics of chemisorbed ammonia

Under conditions of low-pressure studies the equilibrium partial pressure of ammonia at elevated temperatures is so low that it is not possible to study its properties in the adsorbed state. At high pressures its abundance on the catalyst surface is high and blocks reactive surface sites. This leads to negative formal reaction order of the technical reaction in ammonia. In addition, the promoting effect of potassium was attributed to a lowering of the desorption energy for ammonia reducing thus the negative formal reaction order. For these reasons the interaction of adsorbed ammonia with single crystals of iron was studied in great detail.

Below room temperature ammonia chemisorbs without dissociation on clean iron single crystals. From

LEED data a structural model for the adsorption geometry was derived [31,30] which still lacks quantitative confirmation. Ammonia is bound to iron through the nitrogen atom. On the (110) face it is positioned above the 4-fold hollow site (see Figure 22). In this position orbital contact is possible between the Lewis base nitrogen (sigma lone pair) to the d-states of the conduction band of iron. The Fe-N bond was identified from HREELS data to occur at 420 cm<sup>-1</sup> [131] which may be compared to the Fe-N bond from beta atomic nitrogen on Fe(111) with 450 cm<sup>-1</sup> [121]. Such a bonding interaction is also known from many amino complexes which are all of the sigma donor type. Theoretical investigations of this interaction [132] on an amino iron complex also suggest that the main bonding interaction occurs through the lone pair orbital which was observed in UPS to shift upon bonding relative to the sigma N-H orbital by about 1 eV [30].

The chemisorption energy of ammonia was found to depend sensitively on the surface orientation [31,30,111]. Its average value of 70kJ/mole is indication for the strong iron-nitrogen interaction. The relevant desorption traces which can be used as probes for the iron surface orientation are shown in Figure 24. All peaks exhibit a feature at about 675 K (exact values: 658 K(110), 661 K (100), 676 K (111), 676 K (211)) characteristic of low-coordination surface sites. The open surfaces (111) and (211) show a complex low-temperature peak structure (495 K to 560 K) which was assigned to chemisorption on the high-co-ordination sites. This trend is in agreement with the bonding mechanism as the electron-rich high co-ordination sites will be poorer acceptors for the sigma donor bond of ammonia than the low-co-ordination surface atoms. The desorption of ammonia occurs within the temperature window of the ammonia synthesis which is in line with the observed self-poisoning in the kinetics.

In an earlier study quite different results are reported. These authors [31] also state the same qualitative TDS profiles but report complete desorption below 320 K. Even at 160 K ammonia was reported to dissociate slowly into N and H. The process was found to be inhibited by pre-adsorbed atomic nitrogen. Further it was reported that high temperature annealing in ammonia caused significant faceting of the (100) plane into complex orientations. The observations imply that ammonia reacts with the iron substrate under modification of the geometric and electronic structure. Under practical reaction conditions these effects will be even more dominating as the temperature window of the observations in the single crystal system is of practical relevance and the partial pressure of ammonia is in the range of atmospheres and not in the range of a fraction of 10<sup>-6</sup> of this as in the model experiments. A different degree of nitridation of the iron single crystals (from the sequence of experiments) may also

explain the discrepancy in the temperature scale of the TDS data reported in the literature.

The desorption of ammonia leaves the surface not clean but causes decomposition into several products and at temperatures above 650 K to noticeable formation of iron nitrides [130]. The first intermediate and highly unstable decomposition product was identified by isotope labelling to be  $\text{NH}_2$ . Above 325 K the  $\text{NH}$  species was identified on Fe (110) [30]. This species is significantly more stable and was characterised with a variety of techniques including SIMS [130]. Monitoring the various fragment intensities allowed to see that very little  $\text{NH}_2$  was present on the surface at any temperature whereas with raising temperature adsorbed  $\text{NH}$  grew up on the account of  $\text{NH}_3$ . At 375 K a sharp cut-off in the  $\text{NH}$  intensity indicates the raising activity of the iron surface for complete dehydrogenation of  $\text{NH}_3$  to N and H. The hydrogen recombines and desorbs below 500 K whereas the atomic nitrogen remains stable on the surface up to 700 K. This large difference in stability explains the observation that the decomposition of ammonia is limited by the desorption of nitrogen atoms which was found in several model studies and with polycrystalline catalysts at steady state conversion [133,134,29].

#### 2.1.5.4. Kinetics of nitrogen chemisorption

These experiments are a corner stone in the attempt to understand ammonia synthesis as it was found from macrokinetic modelling as well as from model experiments that nitrogen dissociation is the slowest step in the sequence of reactions leading to ammonia. Several surface science experiments have revealed a great deal of quantitative knowledge about this unusually complex process but a full understanding of the molecular dynamic processes is required in order to ensure that the experimental data obtained at rather special conditions can be safely extrapolated to other conditions over a wide range of parameters and that the observations do not represent special cases caused by the idealised conditions of e. g. gas flow conditions or heat transfer between gas and solid surface.

The fundamental results of chemisorption isotherms of atomic nitrogen on iron single crystals are displayed in Figure 25. The data were obtained at 693 K crystal temperature using a gas dosing pressure of  $4 \times 10^{-4}$  mbar and Auger electron spectroscopy as detection method. Care was taken to consider the presence of dissolved N atoms in these model experiments [26,27]. The samples had to be pre-nitrided before reproducible sorption isotherms could be obtained. Any pre-activation of the

molecular nitrogen by e.g. slow electrons from hot filaments were carefully avoided. Of course, full protection of the system from adventitious CO and oxygen was required which was achieved by the long experiment time (years) in which the UHV system pumped only nitrogen and hydrogen.

The sticking coefficient of atomic nitrogen is very small and depends markedly on the crystal orientation. From the slopes of these curves initial sticking coefficients of  $7 \times 10^{-8}$  (110),  $2 \times 10^{-7}$  (100),  $4 \times 10^{-6}$  (111) at 683 K were determined. The sticking coefficient raises by two orders of magnitude upon changing the surface structure from the densely packed (110) to the open configuration (111) (see Figure 22). It is most significant that exactly the same dependence of the ammonia synthesis turnover frequency was found at 20 atm pressure with single crystals [76]. A constant ratio between the two quantities clearly reveals the direct correlation between atomic nitrogen abundance and ammonia turnover frequency although a pressure gap of 5 orders of magnitude lies between the two sets of kinetic data. In the high pressure work also other surface orientations exhibiting C7 sites were tested for ammonia synthesis activity but the (111) orientation exhibiting exclusively two adjacent rows of C7 site in the surface (see Figure 22) was found to be the most active surface plane. Measurements of the sticking coefficient on technical catalyst samples arrived independently [95] at a value of  $1 \times 10^{-6}$ . The reason for the variation of the sticking coefficient were traced back to a variation of the activation energy for chemisorption ranging at initial coverage from 27 kJ/mole (110), 21 kJ/mole for (100) and 0 kJ/mole for (111). It is noted that these values for initial adsorption increase significantly for higher coverage by about a factor of 2 for 5% coverage [26]. In remarkable contrast are the activation energies for desorption of nitrogen which were determined from an analysis of TDS data. They are also dependent on crystal orientation with values from 234 kJ/mole (110) over 242 kJ/mole (100) to 213 kJ/mole (111) [27].

It was concluded that the molecular alpha nitrogen acts as precursor for the formation of atomic nitrogen. The situation which was analysed quantitatively for the (111) surface [124] is schematically represented in Figure 26. The relevant numerical values for the kinetic constants are collected in Table 4.

Table 4. Kinetic parameters of nitrogen chemisorption on Fe (111) in the limit of low coverage.

	Pre-exponential ( $s^{-1}$ )	Activation energy (kJ/mole)
ads	$10^{11}$	0
des	$10^{10}$	31
rec	$10^9$	146
dis	$10^7$	28

The dissociation of molecular nitrogen proceeds through a weakly held molecular precursor (alpha nitrogen, sticking coefficient  $10^{-2}$ ) and then across an activation barrier into the atomic state. The difference between the desorption energy of the precursor and the activation energy for dissociation which is designated in the Figure as  $E^*$  determines the overall chance of adsorbed molecular nitrogen to remain as atomic species on the surface relative to its desorption back into the gas phase. The experimental value for  $E^*$  on the (111) surface was found to be -3 KJ/mole. The ratio of desorption to dissociation is about  $10^{-3}$  explaining together with the sticking coefficients of alpha nitrogen of  $10^{-2}$  and that of gamma nitrogen which is the precursor to the rate-determining precursor of  $10^{-1}$  the overall low sticking coefficient for dissociative chemisorption. The choice of the alpha nitrogen structure as precursor to the reaction intermediate is strongly supported by the structure-sensitivity of the sticking coefficient. Only the alpha species reacts sensitively on the local geometry of the adsorption site and will bind strongly (lowering the  $E_{des}$  value in Figure 26) on open surfaces exposing electron-rich C7 sites.

The parameters for the recombination of atomic nitrogen indicate the strong interaction of this species with the substrate and illustrate that once the nitrogen is in this deep potential minimum then the subsequent hydrogenation is kinetically facile compared to recombination and desorption.

A comment is needed on the numerical accuracy of the data in Table 5. Besides more trivial problems with co-adsorption and the integrity of surface orientation some more subtle effects affect the validity of the data. First it was found by isotopic exchange reactions [26] that with increasing temperature the contribution of sub-surface nitrogen to the TDS signal increases which changes the „surface“ under study from a two-dimensional object into a three-dimensional object with a thickness depending on temperature, pre-history (filling of the bulk) and heating rate (diffusion kinetics). In addition, the detection method AES is less surface sensitive than the detection method of work function change, which in turn is difficult to calibrate in terms of amount of nitrogen desorbed. The comparison of the response of work function change and AES signal yielded a proportionality for the (100) face but a function of temperature for the (111) face indicating the operation of a structural effect which could be seen as facetting in LEED observations. All these points which were well-discussed in the original work have to be taken into account when estimating error bars.

The combined studies of ammonia synthesis [109, 110] and chemisorption of nitrogen [26,27, 124] on several faces of iron single crystals yielded an internally consistent picture about the mechanism of ammonia synthesis which can explain on an atomic level the nature of the rate-determining step, the mode of action of the catalyst and the structure-sensitivity of the reaction found in several model studies on polycrystalline catalysts. In addition, the data were proportional for various surface orientations over 5 orders of magnitude in nitrogen pressure suggesting that the kinetic data of the UHV model experiments should be suitable explain the high pressure kinetic data at least over single crystals. To extend the validity of such a quantitative model the following assumptions must be made:

- The surface structure of polycrystals and single crystals must be essentially the same ((111) patches on the polycrystalline catalyst)

- The effect of the alkali promoter on the elementary steps must be understood (and the contribution of all the other promoter species present must be excluded). A set of experiments with alkali promoted single crystals is needed.

- No qualitative change in the rate-determining step as function of pressure must occur. Polycrystallinity or possible different surface electronic structures may not interfere with the energetics and kinetics of the molecular and atomic nitrogen species.

- The inhibiting effect of the product ammonia has to be taken into account. At high conversions a significant site blocking effect will affect the experimental turn-over.

- Under practical reaction conditions all reactions except the rate determining step are to be treated in equilibrium requiring a second set of kinetic data for the backward reactions.

The key process of dissociative nitrogen chemisorption was tested for its dependence on the kinetic energy of the incoming molecules. The idea was that the precursor model may be valid only as a limiting case at low kinetic energies of the gas molecules and the sticking coefficient could be significantly different at higher energy contents of the nitrogen molecules. In conventional theories [135] of dissociative chemisorption with low overall probability the barrier for the atomic state lies above the energy of the unbound molecule as sketched in Figure 26 top. The case of nitrogen on iron is special, as the bottle neck is not only the dissociation but the formation of the precursor. With increasing energy of the molecules the bottle neck will become more important but the process of dissociation might be facilitated.

In a series of molecular beam experiments [136] with molecular nitrogen and Fe (111) at 520 K the kinetic energy of the nitrogen molecules was varied in the range of 0.05 eV to 5 eV by varying the nozzle temperature between 300 K and 2000 K. A dramatic change of the sticking coefficient from the value determined by the conventional technique up to about 0.1 at about 3 eV kinetic energy was observed. This observation alone would cast doubt on the relevance of the precursor state for the overall process and a direct pathway from molecular to atomic nitrogen could be deduced. In a further series of experiments at constant kinetic energy the crystal temperature was varied and a significant increase of the sticking coefficient was found with decreasing temperature. This observation is in even quantitative agreement with the conventional chemisorption experiments [33] and implies that even at kinetic energies which are high relative to the practical ammonia synthesis temperature the substrate temperature is of importance which can be seen as a strong argument against a one-step dissociation model. With a combined sorption and desorption experiment it could be shown that the alpha state identified in the conventional chemisorption experiments is also involved in the variable kinetic energy chemisorption. Moreover, the sticking coefficient into the alpha state was shown to increase with increasing kinetic energy from 0.05 at 1.0 eV to 0.12 at 3.9 eV and a crystal temperature of 120 K. Further evidence against a one step mechanism is the observation that the saturation coverage

in nitrogen is not dependent on the kinetic energy of the molecules as it was observed for the one-step dissociation of nitrogen on W (110) [137,138]. Keeping in mind that even at the most dense atomic nitrogen structure observed (see Figure 23) would allow for a more dense atom packing in the adlayer form geometric arguments, it was concluded that the atoms forget about their energetic history as they are formed over the energy barrier from the precursor state. The specific suitability of the (111) orientation of iron for the precursor mechanism is further illustrated by the fact that the same molecular beam experiment with variable kinetic energy using Fe (110) as target did not bring about the strong variation of the sticking coefficient with kinetic energy [139] which is a strong argument against the one-step mechanism

In summary, the series of molecular beam experiments strongly support the view that the precursor mechanism of nitrogen chemisorption will also hold under practical synthesis conditions. The authors of ref. [136] conclude from the dependence of the sticking coefficient on kinetic energy of molecular nitrogen that not only alpha nitrogen but possibly other specific configurations with a modified chemisorption energetics are also involved as precursors. The molecular beam studies do not, however, give any evidence for the one-step mechanism or other not precursor-mediated pathways of nitrogen dissociation as it was incorrectly concluded in an account on the nature of nitrogen dissociation [140].

#### 2.1.5.5. The effect of the potassium promoter

Understanding the effect of the electronic promoter alkali (exemplified for potassium as the most studied species) on the elementary steps of ammonia synthesis [141,46] is a further prerequisite to extrapolate surface science data into macrokinetic models. The surface of an activated catalyst is covered with significant amounts of alkali [82, 92, 94, 93] and it is known since early days [46, 142] that this coverage is very beneficial for the catalyst performance as it modifies various steps in the sequence of elementary reactions [11,143,144, 125] in the overall process. The phenomenon is rather common in catalysis and has provoked a large body of theoretical and experimental work [145]. Although it was shown that under reaction conditions the catalyst must contain a unique surface oxygen-alkali species („K+O“) [146,147] the fundamental study [148] was done with pure potassium on iron single crystals and the effect of the presence of essential stabilising oxygen was concluded to be of quantitative rather than to be of qualitative nature (it decreases the efficiency of the promoter which is in agreement with model studies under practical reaction conditions [149]). The results described here are supported without a detailed

discussion by a body of spectroscopic work on the K+O+Fe interaction [150,151].

The presence of fractions of a monolayer of potassium cause the occurrence of a second desorption feature for the alpha nitrogen molecule which is more tightly held with a difference in chemisorption energies from 31 kJ/mole for bare Fe (111) to 48 kJ/mole for potassium covered iron. A comparison of TDS data and LEED measurements for Fe (100) and Fe (111) leads to the following conclusion:

- With increasing K coverage the abundance of the new alpha 2 species grows on the expense of the original alpha 1 form.

- Both species adsorb and desorb independently and do not exchange during the heating of the TDS experiment.

- The energetics of the atomic N species is qualitatively not affected by the presence of potassium besides a site blocking for large potassium coverages. In particular, the structural ordering of the Fe-N system is not changed by the randomly adsorbing potassium. This implies that the kinetic effect of the potassium on N<sub>2</sub> adsorption is exerted on a different adsorption site than the final binding of the resulting atomic nitrogen.

- The sticking coefficient for atomic nitrogen on Fe (111) is raised by a factor of 8 to a value of  $4 \times 10^{-5}$  for initial coverage.

- The structure sensitivity of nitrogen chemisorption is lifted upon potassium exposure. The sticking coefficient on Fe (100) and Fe (111) were found to be equal resulting in an enhancement factor of 280 for Fe (100).

- Work function change measurements indicate that potassium interacts strongly with iron being transformed in a cationic species. The iron-nitrogen interaction remains dominant but there is also a potassium-nitrogen interaction levelling off the absolute work function differences on different crystal planes which is in agreement with the identical desorption energy of the alpha 2 state in TDS experiments.

These findings were interpreted in [148] in the following way. Alkali chemisorption increases the local electron density around its adsorption site by charge donation into the conduction band of iron. In their vicinity the bond strength of the alpha nitrogen-iron interaction is increased resulting in the alpha 2 state. Whereby simultaneously the N-N bond is weakened and the activation barrier for dissociation is lowered. The N atoms formed may diffuse away from these sites and eventually spread over the entire surface.

In the context of the precursor model of nitrogen dissociation the different sticking coefficients on Fe (100) and Fe (111) can be rationalised as sketched in Figure 26. The positive activation barrier describes the reaction on Fe (100), whereas the negative activation barrier belongs to the Fe (111) orientation. If for the case of positive  $E_{\text{dis}}$  the value of  $E_{\text{des}}$  is increased by the presence of potassium (increased electron density at the iron binding sites) and the potassium nitrogen interaction is weak enough not to modify the shape of the potential curve then the lowering of the desorption energy will bring down the point of intersection of the potentials for the molecular and the atomic state resulting in a lowering of the activation barrier for dissociation  $E_{\text{dis}}$ .

The complication that the alkali promoter is not present in its pure form but as a co-adsorbate with oxygen is not only unavoidable by the enormous affinity of finely divided alkali towards oxygen [152] but is essential to keep the promoter on the surface. Thermal desorption following co-adsorption reveals [146] a stabilisation from a maximum rate of desorption of 550 K (terminating at 900K) to 750 K (terminating above 1000K). The stabilised form is thus likely to remain stable under practical reaction temperatures. The spectroscopic analysis [151,150] reveals that the interaction of oxygen is primarily with iron which classifies the oxygen as a co-adsorbate and not as a potassium oxide or hydroxide. These findings are rather similar for all crystal orientations of Fe and also hold well for polycrystalline iron foil. At alkali coverages below 10% of a monolayer the alkali is chemisorbed more strongly to the surface [150,146] as consequence of the strong electronic interaction with the substrate at low coverages [145].

In a thorough theoretical analysis of the alkali effect [153, 154] it was shown that in agreement with the experimental facts described the iron-potassium interaction is of a local electrostatic character and not a covalent long-range interaction with re-hybridisation of the alkali s states with the iron d states. Consequently, there is no qualitative difference to be expected if the actual surface situation is not Fe+K+N but Fe +K+N+O+NH<sub>3</sub>. Oxygen will compete



with the less electronegative nitrogen for the extra electron density and thus reduce the total extra electron density available for enhanced alpha nitrogen bonding. This explains the observation of an overproportional decrease in nitrogen sticking coefficient with oxygen coverage of the Fe+K system [146] in contrast to the linear site blocking behaviour found for bare iron [155]. At the coverage ratio between potassium and oxygen of about 1:1 where the promoter remains stable on the surface under practical reaction conditions the electronic promoting effect measured by the initial sticking coefficient has reduced from a factor of 8 for Fe (111) to a factor of 2.

The local character of the electronic modification of iron at the potassium adsorption site is such that it does not affect the nitrogen atoms which are strongly chemisorbed into the top iron surface plane. Would the bonding enhancement also act on atomic nitrogen the promoter effect could well be detrimental as it would contribute to a decreased surface mobility and thus site blocking of atomic nitrogen. This requirement is full in line with the potential diagrams calculated for the iron-potassium interaction [153].

The situation with the co-adsorbed ammonia is characteristic for high pressure operation where the abundance of ammonia and of eventual partly hydrogenated precursor species is significant. The relevance of this additional promoter action can be deduced from the practical observation [47,3] that the potassium promoter action drastically increases with total educt pressure. In low-temperature ammonia TDS experiments [156] it was found that a potassium co-adsorption of about 0.1 monolayers reduced the desorption maximum of molecular ammonia by 40 K to below 300 K. Higher abundances of (nominally oxygen-free) potassium loadings create a new desorption feature at 185 K on the expense of the original broad signal below 300 K. This result was used to infer a destabilisation of the chemisorption of ammonia which should reduce the self-poisoning effect at high conversions.

The assumption was tested in a series of conversion experiments with (111) and (100) single crystals at 20 bar pressure. A nominal half monolayer of K+O was pre-adsorbed and tested to remain present under synthesis conditions. The conversion was found to be enhanced by 30% for normalised surface areas relative to clean iron. The structure sensitivity was not lifted as in the nitrogen chemisorption experiments. No noticeable effect of the presence of potassium on the activation energy for ammonia synthesis was found. The reaction order in ammonia was found to change from -0.6 to -0.35 by the presence of the promoter. These findings [156] were used

to infer that the promoter does not modify the elementary step of ammonia synthesis but rather removes site blocking by the product ammonia. These results are in qualitative agreement with similar observations on a polycrystalline catalyst [147].

The reduced effect of alkali under conversion conditions relative to nitrogen and hydrogen chemisorption [148,33] may be due to the damping effect of co-adsorbed oxygen. The destabilising effect of alkali on ammonia adsorption may be of relevance in situations where very few active sites are available. This situation is typical for the single crystal catalysts which are extremely poor catalysts in terms of efficiency (the ratio between equilibrium conversion and measured conversion) as can be seen from the overall small negative value of the reaction order in ammonia. If catalysts become more efficient the effect of creation of additional precursor sites for nitrogen activation (the alpha 2 site) may be important. Such a mode of action would be full in line with the conjecture that a distribution of precursor geometries exist for nitrogen activation at finite kinetic energy of the nitrogen molecules [136]. The very detailed experimental and theoretical studies of the alkali promotion have revealed a whole suite of possible mode of actions which are all valid in the context of their respective reaction conditions without being able to pin down their relative importance under practical conditions. The analysis of kinetically controlled practical processes by model studies which are bound to be far away in their reaction conditions (kinetic parameters, not temperature and pressure) finds its limits as both the pressure and material gaps preclude kinetic extrapolations on the basis of observations.

## **2.1.6. Nitrogen chemisorption with polycrystalline substrates at elevated pressures**

### **2.1.6.1 Model studies**

The nature of the substrate surface under reaction conditions appears top on the list of possible interferences in extrapolating the single crystal data to polycrystalline catalysts. The following considerations were put in this separate section as under high pressure synthesis conditions the as yet small effects of nitrogen incorporation into the iron lattice will increase significantly. No direct theoretical or experimental data are available as yet to study the possible consequences on the reaction mechanism. For this we have to resort to related observations under still low-pressure conditions which indicate, however, the possibility that the nitrogen incorporation into iron which is a real high-pressure effect may modify our present notion about the mode of operation of the catalyst.

Even under the conditions of the model experiments with iron single crystals it was found that a metastable nitride forms their surface rather than pristine iron. The presence of the nitrogen atoms causes strain in the lattice and modifies thereby the substrate electronic structure [157]. Lattice parameter anomalies were also found with the technical catalyst. Effects of strain on the chemisorption behaviour were reported for Cr (110) layers which became highly active in dissociative nitrogen adsorption at 80 K which is not found on perfect (Cr 110) surfaces [158].

In a series of chemisorption experiments of differently strained iron (110) films on W (111) combined with ARUPS detection of the nature of the adsorbed nitrogen [105] it was found that unstained iron films are fully inactive in full agreement with the single crystal data. As strain increases with decreasing film thickness the amount of molecular nitrogen increases drastically. From ARUPS it could be shown that the species was gamma nitrogen, whereas the TDS characteristics indicate a distribution of sites with a chemisorption energy of about alpha nitrogen. The presence of flat lying molecules was, however, conclusively ruled out for all films investigated. Unexpected was further the observation that nitrogen dissociation began already at temperatures as low as 80 K as revealed by the very sensitive tool of synchrotron ARUPS [127]. The films were fully converted into nitrides already at 300 K exhibiting the LEED pattern of the nitride structure in Figure 23. The nitride exhibits the same thermal stability as atomic nitrogen on single crystals. Unstrained (110) films are almost inactive even at 650 K towards nitridation even at drastic exposures. Most remarkably, the nitrided surfaces are fully inactive for chemisorption of further molecular nitrogen. The surfaces are passivated in the absence of hydrogen which chemically removes the site blocking nitrogen atoms.

These results suggest that in full agreement with the concept of a distribution of precursor geometries arising from the analysis of the molecular beam experiments not only alpha 1 and alpha 2 nitrogen but also gamma nitrogen on strained iron (110) might act as precursor for nitrogen dissociation. Strain not simply „opens“ the surface but leads to a new electronic structure which favours the formation of a strongly held end-on molecular species. This model experiment is further of relevance as it illustrates that purely structural modifications of the surface without the presence of an „electronic“ promoter can severely affect the elementary step of nitrogen adsorption. The distinction between structural and electronic promotion may thus be questionable as coadsorption of e.g. strongly adsorbed atomic oxygen next to an alkali centre may have a comparable effect on the local electronic surface structure than strain. Should the strain promotion of nitrogen

adsorption also work on polycrystalline catalysts, then kinetic modelling using only the parameters for the alpha precursor may be incomplete. It is pointed out that this presently pure speculation which could account for quantitative discrepancies between models and observations (section 2.1.7.) does not affect the fundamental ingredients into our overall picture about the mechanism of ammonia synthesis. The main consequence would be that additional geometric arrangements may describe the local structure of the active sites apart from the (111) and (211) surface terminations.

### 2.1.6.2. Polycrystalline catalyst substrates

Here two main issues dominate the experiments. First an analysis of the average surface orientation would be desirable in order to show that also in these systems the thermodynamically metastable (111) facet is present and the alpha state molecular nitrogen precursor mechanism can be applied in kinetic modelling. Further it needs to be shown that the single crystal faces are stable with respect to restructuring under the influence of the high partial pressure of ammonia (nitrides) and of structural promoters. Finally, the parameters of the elementary step reactions determined in the limit of low pressure, low conversion and low density of active sites should be tested for effects of finite to large coverages and higher densities of active sites.

The first task was accomplished by performing TDS experiments on a sample of fully reduced [47] technical ammonia synthesis catalyst. In the reference experiments on Fe (111) it was clearly found that potassium promoted (111) faces exhibit a characteristic TDS pattern [148,125] with three peaks for gamma, alpha 1 and alpha 2 molecular nitrogen. As the molecular precursor species and not the surface orientation are the most relevant features for the kinetic analysis it was felt that if the technical catalyst would exhibit the same TDS pattern from low temperature nitrogen adsorption this experiment will contribute to bridge the material gap between single crystals and polycrystals. The experiment was successfully performed [159] and for a special combination of parameters excellent agreement in the TDS patterns between the two systems was observed.

In Figure 27 N<sub>2</sub> TDS data are displayed for a technical catalyst which was fully activated and tested to produce ammonia before the experiment. The good agreement between the patterns recorded for the two possible signals for nitrogen (left pattern in Figure 27) excludes significant interference with possibly co-adsorbed CO. At a heating rate of 5 K/s perfect agreement is obtained in shape and position for all three species with

single crystal data (dashed lines in the Figure). Systematic variation of the heating rate revealed that the gamma peak is insensitive in position to this parameter as it is expected for the desorption of a molecular species. This is clearly not the case for the alpha species as can be seen from the right pattern of Figure 27. The behaviour implies that the alpha species dissociate and desorb via recombination without, however, thermally activated exchange between the two alpha states as it was already found with the single crystals [148]. It is pointed out that the two alpha species were also observed in TPD experiments at atmospheric pressure [85]. In this work the desorption features deviated much more significantly from the single crystal data than the features shown in Figure 27. The other catalytic data given in this work suggest that the catalytic performance was indeed inferior to those observed for the samples of Figure 27 [47]. A correlation between catalytic performance and energetic parameters of the precursor state is expected to hold if the dissociation of nitrogen is indeed the *rd*s in ammonia synthesis.

The structural modification of iron by ammonia was already concluded from the beneficial effect of iron oxide reduction by synthesis gas rather than by pure hydrogen. Using single crystals of Fe (100), (110) and (111) orientations it was shown that all three surfaces facet into polycrystalline surfaces after treatment with ammonia at 723 K and 5 mbar pressure for 30 min [160]. The facets were large enough to be seen with the SEM [107]. They all generated or enhanced the abundance of the (111) orientation as can be concluded from the shape of the facets. Using ammonia TPD as structure sensitive probe, it was found that indeed on all three surfaces the desorption feature from C7 sites occurred. Conversion experiments showed a large increase in activity for the nominal (100) surface and activation of the initially fully inactive (110) face to about 30% of the activity of untreated (111) iron. It was further found that pre-treatment with ammonia enhanced the nitride content of the surface considerably from 9% surface coverage to 60% coverage without finding, however, a correlation between nitride content and catalytic activity. It was concluded that the nitrogen should reside as sub-surface species on the iron and remain inaccessible for surface reactions. This observation suggests that the nitride formation is responsible for the faceting or the stabilisation of the facets. On (111) surfaces the interstitial nitride species can be structurally accommodated very easily (see Figure 23) and under ammonia partial pressure elemental iron is metastable against nitride formation (see section 2.1.3.2). In the light of the sensitivity of the nitrogen dissociation mechanism for lattice strain [105] this finding may be significant as under practical reaction conditions not pure iron but always nitrogen-intercalated iron with the respective lattice strain is present [62,23].

The chemisorption of molecular nitrogen at atmospheric pressure over technical catalysts was studied by several authors with calorimetric and temperature-programmed desorption techniques. These studies directly probe the elementary step which is the bottle neck of the overall process and are of key importance for a mechanistic understanding.

An early study by Emmett and Brunauer [95] revealed isotherms at 723 K which are incompatible with the Langmuir expression but were well explained by Freundlich isotherms. From an analysis of the data the activation energies of adsorption, desorption and the heat of dissociative nitrogen adsorption were derived. The largest energy barrier was found for the nitrogen desorption in quantitative agreement with a study of nitride decomposition [29]. It was finally concluded that the „rate of nitrogen adsorption is in the right magnitude to be the slow step in ammonia synthesis“.

A very detailed and accurate gravimetric study was carried out by Scholten and co-workers [28] and was used by many different authors for comparison or support for their own results. They found that the activation energy for nitrogen adsorption is not constant but increases with coverage. From zero coverage up to a critical value of 0.22  $\Theta$  the adsorption energy rises on this alumina promoted low-surface area catalyst from 22 kJ/mole to about 90 kJ/mole. At higher coverages only a slight change to 96 kJ/mole was measured. The activation energy for desorption changed linearly with coverage from 230 kJ/mole for zero coverage to 127 kJ/mole at full coverage. Using the relation by Emmett and Brunauer [95]

$$Q_{\text{ads}} = E_{\text{des}} - E_{\text{ads}}$$

it follows that the heat of adsorption is a non-linear function of coverage with values from 170 kJ/mole to below 50 kJ/mole. It is noted that these data are far higher than the values determined from single crystal experiments (see section 2.1.5.2). This was attributed by several researchers to the presence of surface impurities such as oxygen on the polycrystalline catalyst (see below).

Recently, two independent studies were carried out with polycrystalline catalysts and nitrogen chemisorption conditions at atmospheric pressure using a microreactor and a mass spectrometer as universal detector [161,162]. Both sets of experiments gave similar results which were interpreted, however, quite controversial. The main results are summarised in Figure 28 taken from ref. [161]. Nitrogen TPD spectra are shown

after steady state ammonia synthesis at 670 K (A) and 600 K (C) respectively. The traces B, D were recorded without pre-dosing nitrogen and indicate quite clearly the presence of bulk-dissolved nitrogen in the activated catalyst which is an independent confirmation of the structural analysis discussed with Figure 20.

The adsorbed nitrogen can be used to determine the number of active sites by conversion of the adsorbed nitrogen into ammonia during a temperature programmed reaction experiment in hydrogen. The result on a triply promoted catalyst was 94  $\mu\text{mole/g}$  active centres assuming a stoichiometry of Fe:N of 1:1. This value transforms to an active surface area of 8  $\text{m}^2/\text{g}$  with a BET total surface area of 21  $\text{m}^2/\text{g}$ . The catalyst exhibits a high fraction of active surface which is in the order of magnitude of earlier measurements [163,95]. This value corresponds to an integral under the nitrogen TPD including the high temperature contributions up to the point where the bulk dissolution sets in.

The TPD traces A, C in Figure 28 exhibit several contributions which must all be attributed to surface species accepting the quantification of the active surface area. If only the recombination reaction of beta nitrogen is assumed to contribute to the TPD signal, a single peak can be fitted well to the leading edge of the TPD profile as shown with trace (E) in Figure 28. This fit assumed a CSTR reactor model and the microkinetic model developed by Stoltze and Norskov [164]. The kinetic parameters of the second-order desorption processes of  $10^{-9}\text{s}^{-1}$  for the pre-exponential and 146 kJ/mole are in excellent agreement with the data in Table 5. It can also be seen that a significant portion of the desorption signal is not accounted for by this model. In order, to investigate the origin of this contributions variations in heating rate and initial coverage tested in TPD spectra. Reduced initial coverage led to a loss of the single peak and left only the broad feature with a peak maximum shifting to higher temperatures with lower coverage. Increasing the heating rate by a factor of 10 increased the abundance of gas phase nitrogen in the desorption maximum by an order of magnitude and increased the contribution to the broad feature relative to the single peak.

Having excluded the segregation of bulk nitride nitrogen to the surface which occurs at higher temperatures [6] two alternative explanations remain:

- The surface is anisotropic in adsorption sites, chemically different adsorption sites exist with different local energetics. The width of the structure calls for a

distribution of site types rather than for few discernible site types.

- The non-negligible partial pressure of molecular nitrogen causes re-adsorption. The porous nature of the catalyst bed and the meso-porosity of the catalyst material allow to account for this deviation from the assumptions for a TPD experiment which simulates better the steady-state situation than single crystal UHV studies, in which only single peak TPD spectra were observed.

Using the reactor model Muhler et al. attempted a quantitative analysis of the whole TPD spectrum choosing the second explanation. The model describes the process sketched in Figure 26. In order to account for the re-adsorption contribution the activation energy barrier between the precursor and the atomic species was assumed to depend on coverage. In this way a linear transition between the extreme cases shown in Figure 26 was built into the model. A set of good fits was obtained using for the activation barrier  $E^*$  in Figure 26 the expression.

$$E^* = -15 + (30 \times \Theta) \text{ (kJ/mole)}$$

where the parameter 30 kJ/mole was determined from the fits. A similar technique was used much earlier by Brunauer et al. [165] to interpret the analytical kinetic equation for ammonia synthesis in terms of a surface heterogeneity with a linear dependence of the activation energy of nitrogen adsorption from coverage.

Under steady state conditions in the limit of high coverage, the adsorption of nitrogen is thermally activated in contrast to the situation described by the parameters of Table 5 which hold for the limit of low coverage as they are extracted from initial sticking coefficients. The value of the activation barrier is significantly lower, as the 96 kJ/mole given by the earlier work [28] determined on a non-potassium promoted catalyst. The model fits almost exactly with early data by Emmett and Bunauer [95] who attributed the observations to the first explanation with a distribution of adsorption sites.

Exactly this interpretation was also chosen by Fastrup [162], who used, in addition to the TPD technique, temperature-programmed adsorption experiments showing the whole sequence of events from adsorption of molecular nitrogen at low temperature to desorption of alpha nitrogen as shown in Figure 27 and the

sorption at high temperature followed by the desorption above 500 K. The richly structured features complement very well the data of Muhler et al.. Despite this good experimental agreement, which is not trivial in the light of the dispute in the literature [166,143], a number of arguments were put forward to support the notion about the site inhomogeneity. The most important conclusion would be that under these circumstances the microkinetic models assuming Langmuir adsorption processes would be inadequate and the chemisorption would have to be described by the Temkin-Frumkin isotherm type.

Of great importance for the validity of the experiments is the exclusion of poisoning effects [167] which was given by the two studies in the limits of detection by the kinetic response. In a detailed photoemission study of nitrogen chemisorption on iron foil [168] a shift of the nitrogen binding energy of atomically adsorbed nitrogen of 0.9 eV was noted after deliberate co-adsorption of oxygen. In the presence of surface oxides the substrate is chemically heterogeneous. Sub-monolayers of oxygen bound to iron could thus well account for the explanation of Fastrup. Although the presence of kinetically detectable amounts of oxygen was excluded [167] the iron catalyst was certainly not homogeneous in the sense of an oxygen-free surface. Besides non-reducible promoter oxides also the potassium promoter requires for its stabilisation the presence of oxygen mainly interacting with the alkali (see section.2.1.5.5). Nitrogen 1s spectra from an in-situ reduced triply promoted catalyst also revealed a broad emission signal for the atomic species indicating a distribution of binding energies.

The argument of interference of oxygen with nitrogen TPD data was already put forward in the context of low-temperature TPD work [166,143,47]. In order to clarify the oxygen presence on reduced polycrystalline catalysts a sample of triply promoted technical catalyst was activated according to technical conditions and operated for 200 h under steady state where it produced at ambient pressure and 600 K 26  $\mu\text{mol}$  ammonia /gs. Then the catalyst was passivated and transferred to the in-situ photoemission system. A sequence of re-reduction experiments was carried out and observed by XPS and UPS. The procedure was chosen as it was found in extensive pilot experiments that it was not possible to fully reduce the catalyst from the oxide precursor under in-situ conditions, a finding which underlines the importance of a sufficient ammonia partial pressure in the final stages of activation [41,96], (section 2.1.4.1). The data are summarised in Figure 29. It can be seen that three successive treatments in hydrogen at 773 K and 500 mbar pressure for 24 h were required to produce an iron 2p line which indicates pure elemental iron besides a small contribution of trivalent iron from the non-

reducible oxides. The structure at 709 eV was also observed with the oxygen-contaminated iron foil [168] and gave rise to the shifted nitrogen spectrum. Although this state of the surface is less-oxygen-contaminated than in earlier experiments [47,94,54], the corresponding UPS data in Figure 29 reveal that the surface is still covered with significant amounts of oxidic components. The structure at the Fermi edge indicates the degree of metallic iron, the line at 5.5 eV arises mainly from oxygen 2p contributions. It can be seen that the re-reductions change the surface iron only moderately (loss of the crystal-field split components of divalent iron oxide at 1 and 3 eV) and act mainly on the sub-surface part of the sample. The relative height of the features can not be taken as indication for their abundance as large and difficult to quantify cross section variations determine the spectral response of such a heterogeneous surface. The data do show that even under drastic reduction conditions of the technical catalyst there is still enough oxygen on the surface to allow for a heterogeneity of the active sites.

The possible source of structural heterogeneity can be excluded by the narrow desorption profile of atomic nitrogen. From single crystal experiments (see section 2.1.5.2) it is known that a spread of 100 K exists between (100), (110) and (111) faces for the atomic nitrogen desorption. The quality of the fits in ref. [161] excludes the presence of significant amounts of a second surface orientation. These data support the conclusion from the low-temperature molecular nitrogen TPD data that only one orientation namely the (111) orientation is dominant in polycrystalline catalysts.

In relation to the single crystal experiments the TPD maximum on the technical catalyst samples occur at almost 200 K lower temperature. Besides the effect of incomplete coverage at the temperature of the desorption maximum the presence of the promoter potassium must be taken into account. This was highlighted in the work of Fastrup showing a difference of about 100 K in the low-temperature TPD maximum for doubly and triply promoted catalysts. Unfortunately, there are no single crystal experiments available which address this point in detail. The effect shows that the alkali promoter directly affects the elementary steps of ammonia synthesis.

### 2.1.7. The mechanism of ammonia synthesis

A detailed understanding of the mechanism of a chemical reaction is the ultimate goal of the catalysis scientist which will allow to give guide lines to the catalysis engineering which can go into a catalyst „design“ [169]. It is pointed out that a direct observation of a reaction mechanism of a

heterogeneous reaction is at present not possible. The quantitative analysis of experimentally determined reaction parameters such as pre-exponentials and activation energies for forward and backward reaction of the analytically determined *vari* and its linking to thermodynamic data such as equilibrium constants using a reaction model which is often referred to as „mechanism“ is the maximum knowledge we can attain at the moment. For a fundamental approach we would require detailed information about the reactant dynamics and the details about energy transfer in the system which is not available yet in any detail.

Most of the published work on ammonia synthesis revolves around kinetic aspects of the reaction. The monographs mentioned in the introduction (in particular the book of Nielsen) give exhaustive and numerically complete reviews about this work. Here a synopsis and the link with the catalyst nature is the aim, not a full review on the subject which can be found for example also in reference [15].

The section refrains from a description of the work on ruthenium [170] as catalyst. A critical account on the actual situation can be found in a review [10]. The interaction of hydrogen is significantly stronger with ruthenium than with iron giving rise to a hydrogen inhibition at low temperatures. From the material side the situation is also more complex as no fused ruthenium catalyst can be employed. Highly dispersed supported systems have to be used which render the definition of a suitable model system difficult. The reaction is structure-sensitive in the sense that a suitable particle size with unknown surface orientation is most efficient. Also the role of the essential promoter alkali is not clearly distinguished as either electronic or structural. The field is under intensive actual exploration with the relevant data on both the surface science and the microkinetic side emerging in the near future.

The necessity to disperse the ruthenium on a support creates additional variables of metal-support interaction and location and location of the promoter either on the support or on the active metal. The very active group of Aika used recently alumina and magnesia as supports besides the traditional support of graphitic carbon. The oxides being acidic and basic respectively in their Brønsted reactivity yielded a set of catalysts in which the synergy of the additional variables could be studied. In addition, these supports allowed to apply infrared spectroscopy to monitor the state of the adsorbed nitrogen at low or ambient temperature. From the discussion of section (2.1.5.2) it appears that the observation by infrared under the experimental conditions of low temperatures and several millibars nitrogen pressure concerns the alpha

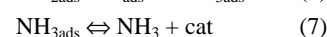
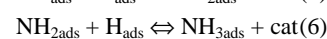
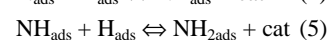
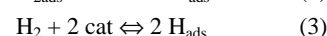
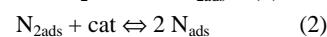
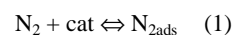
molecular species with its end-on bonding geometry. In Figure 30 it is illustrated that a striking correlation exists between the N-N bond strength of the precursor state and the steady state catalytic activity. The finding that lower N-N- bond strength correlates with higher catalytic activity is a good confirmation of the mechanistic picture with the activation of molecular nitrogen being the *rds* in ammonia synthesis. The data show that the more Brønsted basic is the oxidic environment the lower is the N-N bond strength. The interpretation of this finding in terms of structure-sensitivity of the activation on the metal (different metal support interaction causes different surface geometry) and several models of the alkali promoter effect is complicated and not yet fully conclusive [171,172,173,174].

### 2.1.7.1 Basic kinetic information

In the period between 1935 and 1979 an extensive body of information was accumulated about the progress of the ammonia synthesis reaction over iron. It is pointed out that none of this information was available to Mittasch when he optimised the catalyst system.

It was assumed that ammonia synthesis occurs via dissociative chemisorption of nitrogen with subsequent hydrogenation of surface atomic nitrogen. The alternative [175] of a successive hydrogenation of chemisorbed molecular nitrogen was also suggested [53] in an attempt to explain the structure-sensitivity of the reaction. Corroboration came from an isotope labelling study of the intermediate hydrazine which was dehydrogenated over polycrystalline iron to unscrambled molecular nitrogen despite of the fact that the N-N bond is weaker than the N-H bond [176]. This notion was controversially debated then and fully rejected after the advent of the single crystal studies described in sections 2.1.5.2 and 2.1.5.4.

The reaction model which was derived from the early kinetic data was based upon indirect conclusions and comprised the following steps.



The term „cat“ designates an active centre at the catalyst surface. From early kinetic work it was known that ammonia synthesis is about as fast as nitrogen chemisorption/dissociation (steps 1,2) which was thus assumed to be rate-determining [141,24177,178]. In successive work analysing the nitrogen chemisorption in context with the ammonia synthesis kinetics [163,95] a low sticking coefficient for dissociative nitrogen adsorption and a significant activation energy for the process (67 kJ/mole) were found as strong supporting evidence for the conjecture that steps (1,2) are rate-determining. Measurements of the heat of adsorption of molecular nitrogen on iron films gave significant lower values (21 kJ/mole) [25] supporting the view that step (2) is rate-determining.

A correlation between face specificity of nitrogen adsorption (even in the molecular state as shown by isotopic marker experiments [25]) and the ammonia synthesis activity was established [179] in line with the findings about structure-sensitivity established by the model experiments of Boudart et al. (see section 2.1.4.1).

The isotopic marker technique applied extensively to ammonia synthesis by the group of Ozaki et al. [24,180170] suggested that chemisorption of nitrogen up to temperatures of 630 K was molecular whereas chemisorption at higher temperature was atomic.

### 2.1.7.2. Analytical rate expressions

This accumulated knowledge about the mechanism was accompanied by a series of developments of analytical rate equations. The prototype equation

$$r = k_A P_{N_2} \left( \frac{(P_{H_2})^3}{(P_{NH_3})^2} \right)^a - k_B \left( \frac{(P_{NH_3})^2}{(P_{H_2})^3} \right)^{1-a}$$

was derived by Temkin and Pyzhev [5] for the limit of high nitrogen coverage relevant under high pressure conditions. The heart of this equation is the replacement of a Langmuir isotherm for nitrogen by a Frumkin isotherm which assumes a heat of adsorption which changes linearly with coverage. The derivation started from the results of ammonia decomposition over iron foil [29] which led to an activation energy for nitrogen desorption by a factor of 2 above the experimental value. To overcome this problem, the concept of energetic heterogeneity of the surface was introduced. This concept

assumes a relation between kinetics (activation energies) and thermodynamics (heat of adsorptions) as was explicitly stated by the authors. It was found by applying the rate equation to differently prepared catalyst that the addition of alkali promoters made the concept working over a wide range of experimental parameters indicating that the concept was more than pure formal description of the kinetics of ammonia synthesis.

The Temkin parameter  $\alpha$  determines to which extent the linear change of the heat of adsorption affects the activation energy for adsorption and desorption of nitrogen.

The development of the analytical rate equations for other boundary conditions such as low coverage of nitrogen or the change in *mari* from atomic nitrogen to NH (step 4) were reviewed by Nielsen et al. [181] and merged into a universal rate equation

$$r = \frac{k_A''' a_{N_2} - k_B''' (a_{NH_3})^2 / (a_{H_2})^3}{\left[ 1 + K_C''' (a_{NH_3}) / (a_{H_2})^g \right]^{2\alpha}}$$

This equation included gas fugacities instead of pressures and removed the pressure-dependence of the rate constant. By fitting the six parameters of this rate equation to a large set of experimental data which forms the test material for all later derived kinetic models [182] the following conclusions could be derived.

- The stoichiometry parameter  $\gamma$  was consistently significantly larger than 1 and was fixed finally to 1.5 indicating that not NH (step4) but N is the *mari* as atomic hydrogen is not involved in the rate determining step ( would mean that  $\gamma$  takes the value 1). This conclusion agrees with the findings of a detailed analysis of the ammonia synthesis kinetics by Boudart et al. [180] who discussed in particular the problem of a much disputed kinetic isotope effect of deuterium on ammonia synthesis [183].

- The Temkin parameter  $\alpha$  was consistently found to be significantly larger than 0.5 with a best value of 0.75 indicative of a sensitivity of the activation energy of nitrogen adsorption upon coverage whereas the nitrogen desorption energy should be less affected by the nitrogen coverage.

- The catalyst surface was assumed to be strongly non-uniform which led the authors to the speculations that the surface behaves dynamically under reaction conditions (modern term „restructuring“) and that the formalism of a single rate-determining step may be inappropriate taking into account a wide „energy spectrum“ of the activated surface.

- The rate equation covered a wide range of pressures and high temperatures up to the thermodynamic limit but failed to explain low-temperature data at and below 600 K.

The success of this empirical rate equation which is the basis of all technical calculations [39] can be seen from the top panel in Figure 31. This figure is reproduced from ref. [182] and shows in a sensitive presentation the correlation of reaction models with the experimental observations from Nielsen [181]. It was pointed out [182] that this rate equation also fits well the data of Ozaki et al. [180] which were taken at low pressures and with a different catalyst sample.

### 2.1.7.3. Microkinetic models

Whereas for practical catalytic purposes the analytical rate expressions are fully adequate their empirical nature with only indirect correlation to observed physical facts was felt to be dissatisfactory. In order to directly use surface physical and quantum chemical data attempts were made to derive rate equations which are not based upon fitting experimental observations but upon calculations using a reaction model and predetermined kinetic and energetic parameters of the reactants. Two families of models were derived by two groups which will be designated as model I [184,164,185,186,49] and model II [187,188,189]. The first report about model I created the term „pressure gap“ and caused considerable interest also outside the catalysis community.

It needs to be pointed out that both models essentially use the reaction model derived by Ertl [190] which is schematically shown in Figure 32. It summarises the energetics of the reaction mechanism qualitatively used for the analytical rate equations. Figure 31 shows that both model families do an excellent job in explaining the practical observations by using parameters which were determined at pressures nine orders of magnitude lower than the extrapolations. It can also be seen that both model families are about equal in their predictive power and differ in their value very little to the remote observer irrespective of the dispute about their quality conducted by the two

groups [191,187]. The presentation of the results chosen for Figure 31 more clearly represents the success of the bridge over the pressure gap than the presentation in Figure 1 which describes the same facts.

The model I explicitly assumes the reaction sequence depicted in Figure 32 and takes the dissociation of nitrogen as the rate-determining step. It assumes all reaction steps except step 2 in the sequence of elementary steps noted above as being in thermodynamic equilibrium and that a treatment according to the Langmuir-Hinshelwood formalism (with fixed heat of adsorptions and uniform sites) is adequate. The model was developed assuming that the expected rate can be predicted from the following input data: (I) the equilibrium constant for the net reaction and all reaction steps except those for the activation of nitrogen, (II) the total gas pressure and (III) the product of the equilibrium constant for molecular nitrogen adsorption with the rate constant for the adsorption of atomic nitrogen (forward reaction of step 2). The heat of adsorption of nitrogen was assumed to be constant with a value of 170 kJ/mole derived from TPD data of Fe (111) single crystals (see sections 2.1.5.2 and 2.1.5.5). The detailed procedure and the parameters chosen can be found in the literature [192,185,49].

The model II takes into account all reaction steps of model I and in addition considers explicitly the molecular and dissociative adsorption of hydrogen in full analogy of the nitrogen activation. The model further includes no assumptions on the rate-determining step and uses no thermodynamic equilibria for the elementary steps but takes experimental rate parameters (pre-exponential and activation energies) from surface science data. One key result of this way of treating the problem is that the rate-determining step comes out as step (2) and that  $N_{\text{ads}}$  is the *major* species in perfect agreement with model I. The heat of adsorption of atomic nitrogen also was assumed constant with a value of 213 kJ/mole which was suspected to be responsible for the systematic underestimation of the reactor output. This underestimation is, however common to both models as can be seen from Figure 31.

A very detailed unifying mathematical analysis of both models was performed in order to identify the reasons for success and failures of the two approaches [193]. The result of the analysis was that both models are equally successful in bridging the pressure gap and that minor differences in selection of parameters and in the presentation of the results were responsible for the initially overestimated [187,191] differences between the two models.



The similarity of the results of the two models was traced back [193] to the common assumption of high coverage of atomic nitrogen on the catalyst under high pressure conditions. With this assumption the rate problem reduces to

$$r = k_{-2} \Theta_N^2 \left( K_{eq} \frac{P_{N_2} (P_{H_2})^3}{(P_{NH_3})^2 (P_0)^2} - 1 \right)$$

with  $k_{-2}$  designating the reverse reaction of step 2 or the rate of desorption and  $K_{eq}$  the overall reaction equilibrium constant. The problem then reduces to a correct choice of pre-exponential and activation energy for atomic nitrogen desorption. These are the crucial parameters and have been chosen differently in the two model families. Due to the compensating effect between pre-exponential and activation energy the different parameter choices almost cancelled each other allowing so similar results.

### 2.1.8. Conclusions

Ammonia synthesis is one of the very few heterogeneous reactions in which a quantitative correlation between elementary steps and macrokinetics has been derived. The correlation underlines the value and the justification of the single crystal approach and illustrates how surface science can be fundamental to catalysis science and engineering. The success was made possible to a large extent by the experimental verification of the reaction scheme in Figure 32 using single crystals. Additionally important were the explanations of the mode of action of the potassium promoter and of the structure-sensitivity. The now proven fact that these findings hold quantitatively for the case of polycrystalline catalysts at high pressures is experimentally founded in the observation that the nature of the sites chemisorbing molecular nitrogen is identical on Fe (111) +K and at the technical catalyst. The model system resembles energetically a small portion of the activated catalyst which was, however, not known at the time when the single crystal experiments were conducted.

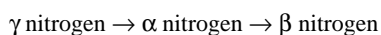
The analysis of the microstructure of the active catalyst has brought evidence that the bcc iron constituting the local structure of all iron structures present has not the consequence of a uniform and homogeneous microstructure. A variety of mesoscopic structural motives ranging from isotropic blocks to platelets with different orientations were found under anaerobic ambient conditions. This variation explains the bi-modal porous structure of the iron crystal as well as it unifies various

experimental observations ranging from paracrystallinity to high resolution TEM data. Traces of nitrogen atoms dissolved in the sub-surface and bulk of the iron were detected. Reference experiments from materials science and thermodynamics predict that the abundance of the interstitial nitrogen atoms causing small deviations of the surface atomic and electronic structure will increase at high pressure ammonia synthesis conditions. As then also the tendency for chemically-induced surface segregation and removal by hydrogenation will also increase, it is as yet difficult to predict how much the active iron surface will be nitrated under steady state conditions. This unavoidable consequence of the high virtual pressure of nitrogen has potential interesting consequences on the abundance of active sites as it was shown in low pressure reference experiments that small lattice distortions of iron can have dramatic effects on its nitrogen dissociation activity. A novel type of active site which exists only at high pressure ammonia synthesis conditions due to the lattice strain of interstitial nitrogen could contribute to the site inventory together with (111) faces of iron platelets which were definitively detected to be present as a minority species in the anisotropic fraction of the iron mesostructures.

The material gap is thus closed as far as the principal occurrence of the structural motif of the model single crystal is concerned. When it comes now with the increasing sophistication of the microscopic understanding to a quantification of the number of active sites per catalyst volume, the consequences of the nitride problem may well have a significant effect on the scaling factors used in present microkinetic models. The experimental uncertainty about the relevance of the nitrides caused inter alia by the kinetic control of their formation highlights the existence of a new material gap where it may have not been foreseen.

The closure of the pressure gap was only possible by the detailed understanding of the microkinetics of each elementary step in this overall simple reaction. The crucial point in this reaction is the dynamics of the atomic nitrogen species on the surface at high coverage. The present status of the modelling suggests that the central bottleneck is the description of both the nitrogen-substrate and the nitrogen-nitrogen interaction which are not adequately represented by fixed energetic terms. All evidence is pointing to the fact that a Langmuir isotherm formalism is only a limiting case describing low-pressure situations. The notion that the extensions introduced into the description of nitrogen chemisorption are exclusively due to adsorbate-adsorbate interactions and that adsorption site heterogeneity can fully be excluded is at present not experimentally founded.

It is the very centre of the pressure gap problem that energetics, kinetics and dynamics of the elementary step nitrogen chemisorption can at high pressures no longer be regarded as single particle to substrate problems but require a detailed and explicit description of the adsorbate-adsorbate interaction. In addition, as the frequency of events is at high pressures much higher than at low pressures, alternative reaction channels which may not represent the global minimum path through the energy hypersurface may become relevant. The reaction sequence



may have other precursor routes leading to  $\alpha$  nitrogen or may even have other precursors to  $\beta$  nitrogen which have not been characterised in their physical parameters as they are in isolated form inaccessible to surface science.

In addition, the energy hypersurface may change shape under the influence of restructuring (nitride formation, spreading of the potassium plus oxygen promoter) and even dynamic responses of the surface geometry at high conversions. The interpretation of the molecular beam studies of nitrogen adsorption [136] and theoretical studies on the dissociation mechanism of nitrogen [194] advocating a tunnelling mechanism are physical equivalents to the intuitive picture of Nielsen et al. suggesting that the active gas-solid interface is „a busy place“ [181].

A comment on the numerical accuracy of the models and their relation to the accuracy of the input values is required. Recently, it was attempted to improve the agreement between models and the very accurate experimental data [186,162,182]. This was done by selecting different input parameters which were available from the significant spread of numerical values reported in the literature and in this article. A particular illustrative example is given in [182] where it was shown that a change in the number density of active sites by a factor of 3 gave almost perfect agreement between model I predictions and the experimental data. Unfortunately, if the surface titration experiments are correct, then a factor of three increase in the number density of active sites would mean that as a conservative estimate each surface site measured by nitrogen low temperature BET would be an active site, a picture which is clearly unphysical. This means that the microkinetic models should not be numerically improved by changing sensitive parameters to more or less justified values as then the difference of the microkinetic approach to the analytical approach gradually vanishes. A decision

about the validity limits of the present models would require a definitive set of input data from surface science which are determined under relevant conditions. The spread in data is not an expression of inaccurate individual experiments but rather an indication about the sensitivity of the results on measurement conditions which were either ill-defined and/or remote from realistic conditions. The generation of a such a data set is, however, a formidable task and its fundamental value may be questionable in view of the principal problems associated with high-pressure mechanisms sketched above.

The reason why the present microkinetic models are both so successful despite this somewhat unsatisfactory experimental situation was pointed out in the analysis of Dumesic [182]. The ammonia synthesis kinetics is most sensitive to the parameters of the nitrogen desorption reaction which are in turn less sensitive to the coverage-dependent effects. This can be seen from the value of the Temkin parameter, as well as from the data of Scholten et al. in the limit of high coverage [195] and from the fit results of Muhler et al. [161]. The emphasis was laid in both models on a correct representation of the TPD data using, however, input data determined in the limit of low coverage which guaranteed a consistent use of the input data. The focusing on the TPD model yielded the largest contribution to the bridge over the pressure gap. The parameters of nitrogen adsorption, on the other hand, are much more dependent on the energy variations with coverage. This can be seen from the modelling attempts of Fastrup [162] using the experimental adsorption data.

The enormous success of the analytical rate expression which stimulates the work on the improvement of the microkinetic models arises from the fact that the coverage dependence of energy is as „heterogeneity“ built into the model. With the advent of experimental data from surface science on coverage-dependent effects the final tuning of the models accounting for the qualitative details of the pressure gap can be expected.

## References

- [1] M. Boudart, Topics in Catalysis. (Eds.: H. Topsoe, M. Boudart, J. K. Norskov), J. C. Baltzer AG, Basel, 1994, Vol. 1, p. 405.
- [2] G. J. Leigh, Acc. Chem. Res., 1992, 25(4), 177-181.
- [3] M. Boudart, Catal. Rev.-Sci. Eng., 1981, 23(1,2), 1-15.
- [4] G. Ertl, Catalytic Ammonia Synthesis: Fundamentals and Practice, Fundamental and Applied Catalysis. (Ed.: J. R. Jennings), Plenum Press, New York, 1991.
- [5] M. Temkin, V. Pyzhev, J. Phys. Chem. (USSR), 1939, 13, 851.
- [6] G. Ertl, M. Huber, N. Thiele, Z. Naturforsch., 1979, 34a, 30-39.
- [7] A. Ozaki, K. Aika, Catalysis, Science and Technology. (Eds.: J. R. Anderson, M. Boudart), Springer Verlag, Berlin, 1981, Vol. 1, Chapter 3, p. 88.
- [8] J. K. Norskov, P. Stoltze, Surf. Sci., 1987, 189/190, 91-105.
- [9] G. Ertl, Angew. Chem., 1990, 102, 1258-1266.
- [10] S. R. Tennison, Catalytic Ammonia Synthesis: Fundamentals and Practice, Fundamental and Applied Catalysis. (Ed.: J. R. Jennings), Plenum Press, New York, 1991.
- [11] K. Urabe, K. Aika, A. Ozaki, J. Catal., 1976, 42, 197-204.
- [12] N. Takezawa, I. Toyoshima, J. Catal., 1966, 6, 145-147.
- [13] M. Boudart, K. Tamaru., Catal Lett., 1991, 9, 15-22.
- [14] C. T. Cambell, Topics in Catalysis. (Eds.: H. Topsoe, M. Boudart, J. K. Norskov), J. C. Baltzer AG, Basel, 1994, Vol. 1, p. 353.
- [15] M. Boudart, G. Djéga-Mariadassou, Kinetics of Heterogeneous Catalytic Reactions, Princeton University Press, Princeton, 1984.
- [16] J. Dumesic, H. Topsoe, S. Khammouma, M. Boudart, J. Catal., 1975, 37, 503-512.
- [17] J. A. Dumesic, H. Topsoe, S. Khammouma, J. Catal., 1975, 37, 503-512.
- [18] F. M. Hoffmann, D. J. Dwyer, Surface Science of Catalysis: In Situ Probes and Reaction Kinetics. (Eds.: D. J. Dwyer, F. M. Hoffmann), American Chemical Society, Washington DC, 1991, Vol. 482, Chapter 1, p. 1.
- [19] A. Mittasch, Adv. Catal., 1950, 2, 81-104.
- [20] A. Mittasch, Geschichte in der Ammoniaksynthese, Verlag Chemie, Weinheim, 1951.
- [21] S. A. Topham, Catalysis, Science and Technology. (Eds.: J. R. Anderson, M. Boudart), Springer-Verlag, Berlin, 1985, Vol. 7, Chapter 1, p. 1.
- [22] K. Tamaru, Catalytic Ammonia Synthesis. (Ed.: J. R. Jennings), Plenum Press, New York, 1991, Chapter 1, p. 1.
- [23] A.M. Vredenberg, C.M. Pérez-Martin, J.S. Custer, D.O. Boerma, L. de Witt, F.W. Saris, N.M. v. der Pers, T. H. de Keijser, E.J. Mittemeijer, J. Mater. Res., 1992, 7(10), 2689-2712.
- [24] P. H. Emmett, K. S. Love, J. Amer. Chem. Soc., 1933, 55, 4043-4050.
- [25] G. Wedler, D. Borgmann, K.-P. Geuss, Surf. Sci., 1975, 47, 592-604.
- [26] F. Bozso, G. Ertl, M. Grunze, M. Weiss, J. Catal., 1977, 49, 18-41.
- [27] F. Boszo, G. Ertl, M. Weiss, J. Catal., 1977, 50, 519-529.
- [28] J. J. Scholten, P. Zwietering, J. A. Konvalinka, J. H. De Boer, Trans. Faraday Soc., 1959, 55, 2166-2179.
- [29] E. Winter, Z. Phys. Chem. B, 1931, 12, 401-425.
- [30] M. Weiss, G. Ertl, F. Nitschke, Appl. Surf. Sci., 1979, 00, 614-635.
- [31] M. Grunze, F. Bozso, G. Ertl, M. Weiss, Appl. Surf. Sci., 1978, 1, 241-265.
- [32] V. I. Tsarev, A. L. Aptekar, V. Krylova, N. S. Torcheshnikov, Reakt. Kin. Catal. Lett., 1980, 14, 229.
- [33] G. Ertl, S. B. Lee, M. Weiss, Surf. Sci., 1981, 111, L711-L715.
- [34] G. Wedler, K.-P. Geuss, K. G. Colb, G. McElhiney, Appl. Surf. Sci., 1978, 1, 471-478.
- [35] K.C. Taylor, J. Catal., 1975, 38, 299.
- [36] R.A. Dalla Betta, J. Catalysis, 1974, 34, 57.
- [37] P. Stoltze, Physica Scripta, 1987, 36, 824-864.
- [38] L. J. Christiansen, Ammonia:Catalysis and Manufacture. (Ed.: A. Nielsen), Springer Verlag, Berlin, 1995, Chapter 1, p. 2.
- [39] J. B. Hansen, Ammonia:Catalysis and Manufacture. (Ed.: A. Nielsen), Springer Verlag, Berlin, 1995, Chapter 4, p. 150.
- [40] M. Hansen, Constitution of Binary Alloys, 2. ed, McGraw-Hill Book Company, New York, 1958.
- [41] H. J. Grabke, Ber. Bunsenges. Phys. Chem. Chem., 1968, 72(4), 533-541.
- [42] J. Schütze, W. Mahdi, B. Herzog, R. Schlögl, Topics in Catal., 1994, 1, 195-214.
- [43] L. Catelliz, W. De Sutter, F. Halla, Monatshefte Chem., 1954, 85(3), 487-490.
- [44] J. Bénard, G. Chaudron, Compt. Rend., 1936, 202, 1336-1338.
- [45] H. Nowotny, F. Halla, Z. anorg. allg. Chem., 1936, 230, 95-96.
- [46] A. Nielsen, H. Topsoe, Catal. Rev., 1970, 4, 1-25.
- [47] W. Mahdi, J. Schütze, G. Weinberg, R. Schoonmaker, R. Schlögl, G. Ertl, Cat. Lett., 1991, 11, 19-31.
- [48] M. Boudart, A. Delbouille, J. A. Dumesic, S. Khammouma, H. Topsoe, J. Catal., 1975, 37, 486-502.
- [49] J. Dumesic, H. Topsoe, M. Boudart, J. Catal., 1975, 37, 513-522.
- [50] M. Boudart, A. W. Aldag, J. E. Benson, N. A. Dougharty, C. G. Harkins, J. Catal., 1966, 6, 92-99.
- [51] R. Van Hardeveld, F. Hartog, Surf. Sci., 1969, 15, 189-230.
- [52] R. Brill, E. L. Richter, E. Ruch, Angew. Chem. Int. Edition, 1967, 6, 882.
- [53] R. Brill, Ber. Bunsenges. physik. Chem., 1971, 75(5), 455-457.
- [54] R. Schlögl, Catalytic Ammonia Synthesis, Fundamental and Practice. (Ed.: R. J. Jennings), Plenum, New York, 1991, p. 19.
- [55] S. R. Logan, J. Philp, J. Catal., 1968, 11, 1-6.
- [56] A. F. Wielers, A. J. H. M. Kock, C. E. C. A. Hop, J. W. Geus, A. M. v. der Kraan, J. Catal., 1989, 117, 1-18.
- [57] P. K. de Bokx, A. J. H. M. Boellaard, W. Klop, J. W. Geus, J. Catal., 1985, 96, 454-467.

- [58] N. Homs, J. L. G. Fierro, A. Guerrero-Ruiz, I. Rodriguez-Ramos, P. R. d. la Piscina, *Appl. Surf. Sci.*, **1993**, *72*, 103-111.
- [59] A. Baiker, R. Schlögl, E. Armbruster, H.-J. Güntherodt, *J. Catal.*, **1987**, *107*, 221-231.
- [60] R. Schlögl, R. Wiesendanger, A. Baiker, *J. Catal.*, **1987**, *108*, 452-466.
- [61] A. Baiker, H. Baris, R. Schlögl, *J. Catal.*, **1987**, *108*, 467-480.
- [62] B. Herzog, D. Herein, R. Schlögl, *Appl. Catal. A*, **accepted 1995**.
- [63] C. Peters, K. Schäfer, R. Krabetz, *Z. Elektrochemie*, **1960**, *64*(10), 1195-1199.
- [64] W. S. Borghard, M. Boudart, *J. Catal.*, **1983**, *80*, 194-206.
- [65] G. Fagherazzi, F. Galante, F. Garbassi, N. Pernicone, *J. Catal.*, **1972**, *26*, 344-347.
- [66] H. Chen, R. B. Anderson, *J. Catal.*, **1973**, *28*, 161-173.
- [67] T. Rayment, R. Schlögl, M. M. Thomas, G. Ertl, *Nature*, **1985**, *315*(6017), 311-313.
- [68] A. Baranski, A. Kotarba, J. M. Lagan, A. Pattek-Janczyk, E. Pyrczak, A. Reizer, *Appl. Catal. A*, **1994**, *General 112*, 13-36.
- [69] A. Baranski, A. Bielanski, A. Pattek, *J. Catal.*, **1972**, *26*, 286-294.
- [70] C. Gleitzer, *Solid State Ionics*, **1990**, *38*, 133-141.
- [71] A. Baránski, J. M. Lagan, A. Pattek, A. Reizer, *App. Cat.*, **1982**, *3*, 207-210.
- [72] A. Baránski, A. Reizer, A. Kotarba, E. Pyrczak, *App. Cat.*, **1985**, *19*, 417-418.
- [73] A. Pattek-Janczyk, A. Z. Hrynkiewicz, J. Kraczka, D. Kulgawczuk, *Appl. Catal.*, **1983**, *6*, 35-40.
- [74] D. A. O. Hope, A. K. Cheetham, G. J. Long, *Inorg. Chem.*, **1982**, *21*, 2804-2809.
- [75] E. R. Jette, F. Foote, *J. Chem. Phys.*, **1933**, *1*, 29-36.
- [76] D. R. Strongin, S. R. Bare, G. A. Somorjai, *J. Catal.*, **1987**, *103*, 289-301.
- [77] H. Schenck, H. P. Schultz, *Arch. Eisenhüttenw.*, **1960**, *31*, 691-702.
- [78] B. B. L. Seth, H. U. Ross, *Trans. Met. Soc. AIME*, **1965**, *233*, 180-185.
- [79] M. Et-Tabirou, B. Dupré, C. Gleitzer, *Metallurgical Trans.*, **1988**, *19B*, 311-317.
- [80] J. Roederer, F. Jeannot, B. Dupre, C. Gleitzer, *Steel Res.*, **1987**, *58*, 252.
- [81] H. Ludwiczek, A. Preisinger, A. Fischer, R. Hosemann, A. Schönfeld, W. Vogel, *J. Catal.*, **1978**, *51*, 326-337.
- [82] P. H. Emmett, S. Brunauer, *J. Amer. Chem. Soc.*, **1937**, *59*, 1553-1565.
- [83] R. Brill, *J. Catal.*, **1970**, *19*, 236.
- [84] H. Topsøe, J. A. Dumesic, M. Boudart, *J. Catal.*, **1973**, *28*, 477-488.
- [85] K. C. Waugh, D. Butler, B. E. Hayden, *Catal. Lett.*, **1994**, *24*, 197-210.
- [86] W. K. Hall, W. H. Tarn, R. B. Anderson, *J. Am. Chem. Soc.*, **1950**, *72*, 5436-5443.
- [87] A. Baranski, M. Lagan, A. Pattek, A. Reizer, *Archiwum Hutnictwa*, **1980**, *25*, 143-151.
- [88] G. Weinberg, B. Beran, M. Muhler, R. Schlögl, A. Dent, T. Rayment, *Appl. Catal. A*, **submitted 1996**.
- [89] G. Fagherazzi, F. Galante, F. Garbassi, N. Pernicone, *J. Catal.*, **1972**, *26*, 344-347.
- [90] R. Hosemann, A. Preisinger, W. Vogel, *Ber. d. Bunsenges. Phys. Chem.*, **1966**, *70*, 797-802.
- [91] R. W. G. Wyckoff, E. D. Crittenden, *J. Amer. Chem. Soc.*, **1925**, *47*, 2866-2876.
- [92] D. C. Silverman, M. Boudart, *J. Catal.*, **1982**, *77*(  
) , 208-220.
- [93] G. Ertl, D. Prigge, R. Schlögl, M. Weiss, *J. Catal.*, **1983**, *79*, 359-377.
- [94] G. Ertl, N. Thiele, *Appl. Surf. Sci.*, **1979**, *3*, 99-112.
- [95] P. H. Emmett, S. Brunauer, *J. Amer. Chem. Soc.*, **1934**, *56*, 35-41.
- [96] P. A. Dowben, M. Grunze, R. G. Jones, *Surf. Sci.*, **1981**, *109*, L519-L516.
- [97] H. Topsøe, J.A. Dumesic, S. Morup, 2, , Academic Press, New York, **1980**, Vol. 2, p. 55.
- [98] J. A. Dumesic, H. Topsøe, M. Boudart, *J. Catal.*, **1975**, *37*, 513-522.
- [99] W. Niemann, B. S. Clausen, H. Topsøe, *Ber. Bunsenges. Phys. Chem.*, **1987**, *91*, 1292.
- [100] H. Topsøe, J. A. Dumesic, M. Boudart, *J. Catal.*, **1973**, *28*, 477-488.
- [101] P. Gallezot, *Catalysis, Science and Technology*. (Eds.: J.R. Anderson, M. Boudart), Springer, Heidelberg, **1984**, Vol. Vol. 5, p. 211.
- [102] R. Buhl, A. Preisinger, *Surf. Sci.*, **1975**, *47*, 344-357.
- [103] V. Solbakken, A. Solbakken, P. H. Emmett, *J. Catal.*, **1969**, *15*, 90-98.
- [104] Z. Paál, G. Ertl, S. B. Lee, *Appl. of Surf. Sci.*, **1981**, *8*, 231-249.
- [105] K. Homann, H. Kühlenbeck, H.-J. Freund, *Surf. Sci.*, **1995**, *327*, 216-224.
- [106] B. Holme, J. Tafto, *J. Catal.*, **1995**, *152*, 243-251.
- [107] D. R. Strongin, G. A. Somorjai, *Catalytic Ammonia Synthesis*. (Ed.: J. R. Jennings), Plenum Press, New York, **1991**, Vol. 4, p. 133.
- [108] L. Wenzel, D. Arvantis, R. Schlögl, M. Muhler, D. Norman, K. Baberschke, G. Ertl, *Phys. Rev. B*, **1989**, *40*(9), 6409-6412.
- [109] N. D. Spencer, R. C. Schoonmaker, G. A. Somorjai, *J. Catal.*, **1982**, *74*, 129-135.
- [110] D. R. Strongin, J. Carrazza, S. R. Bare, G. A. Somorjai, *J. Catal.*, **1987**, *103*, 213-215.
- [111] D. R. Strongin, J. Carrazza, S. R. Bare, G. A. Somorjai, *J. Catal.*, **1987**, *103*, 213-215.
- [112] K. Christmann, *Surf. Sci. Rep.*, **1988**, *9*, 1-163.
- [113] E. Shustorovich, *Surf. Sci. Rep.*, **1986**, *6*, 1-63.
- [114] P. Nordlander, S. Halloway, J. K. Norskov, *Surf. Sci.*, **1984**, *136*, 59-81.
- [115] W. Kinzel, W. Selke, K. Binder, *Surf. Sci.*, **1982**, *121*, 13-31.
- [116] F. Bozso, G. Ertl, M. Grunze, M. Weiss, *Appl. Surf. Sci.*, **1977**, *1*, 103-119.
- [117] E. A. Kurz, J. B. Hudson, *Surf. Sci.*, **1988**, *195*, 15-30.
- [118] J. P. Muscat, *Surf. Sci.*, **1981**, *110*, 389-399.

- [119] M. Grunze, M. Golze, J. Fuhler, M. Neumann, E. Schwarz, *Proc. 8th Int. Cong. on Catalysis*, (Ed.: G. Ertl), Verlag Chemie, Weinheim, 1984, Vol. IV, p. 133.
- [120] M. Grunze, G. Strasser, M. Golze, *Appl. Phys. A*, 1987, 44, 19-29.
- [121] M. Grunze, M. Golze, W. Hirschwald, H.-J. Freund, H. Pulm, U. Seip, M. C. Tsai, G. Ertl, J. Küppers, *Phys. Rev. Lett.*, 1984, 53(8), 850.
- [122] K. Kishi, M. W. Roberts, *Surf. Sci.*, 1977, 62, 252-266.
- [123] D. Tomanek, K. H. Bennemann, *Phys. Rev. B*, 1985, 31(4), 2488-2490.
- [124] G. Ertl, S. B. Lee, M. Weiss, *Surf. Sci.*, 1982, 114, 515-526.
- [125] L. J. Whitman, C. E. Bartosch, W. Ho, G. Strasser, M. Grunze, *Phys. Rev. Lett.*, 1986, 56(18), 1984.
- [126] C. Krüger, Y.H. Tsay, *Angew. Chem.*, 1973, 85, 1051.
- [127] H.-J. Freund, B. Bartos, R. P. Messmer, M. Grunze, H. Kuhlenbeck, M. Neumann, *Surf. Sci.*, 1987, 185, 187-202.
- [128] J. A. Dumesic, H. Topsoe, M. Boudart, *J. Catal.*, 1975, 37, 513-522.
- [129] T. Yamabe, K. Hori, T. Minato, K. Fukui, *Inorg. Chem.*, 1980, 19, 2154.
- [130] G. Ertl, M. Huber, N. Thiele, *Z. Naturforsch.*, 1978, 34a, 30-39.
- [131] W. Erley, H. Ibach, *J. Electron Spectrosc.*, 1983, 31, 61.
- [132] K. Hermann, *Suppl. Le Vide, Cannes*, 1980, p. 196.
- [133] D. G. Löffler, L. D. Schmidt, *J. Catal.*, 1976, 44, 244-258.
- [134] G. Ertl, M. Huber, *J. Catal.*, 1980, 61, 537-539.
- [135] J. E. Lennard-Jones, *Trans. Faraday Soc.*, 1932, 28, 333-359.
- [136] C. T. Rettner, H. Stein, *Phys. Rev. Lett.*, 1987, 59(24), 2768.
- [137] J. Lee, R. J. Madix, J. E. Schlaegel, D. J. Auerbach, *Surf. Sci.*, 1984, 143, 626-638.
- [138] H. E. Pfnür, C. T. Rettner, J. Lee, R. J. Madix, D. J. Auerbach, *J. Chem. Phys.*, 1986, 85(12), 7452-7466.
- [139] J. Böheim, W. Brenig, T. Engel, U. Leuthäusser, *Surf. Sci.*, 1983, 131, 258-272.
- [140] M. Bowker, *Topics in Catalysis*, 1994, 1, 265-271.
- [141] P. H. Emmett, S. Brunauer, *J. Amer. Chem. Soc.*, 1937, 59, 310-315.
- [142] L. A. Rudnitsky, M. G. Berengarten, A. M. Alekseev, *J. Catal.*, 1973, 30, 444-450.
- [143] H. D. Vandervell, K. C. Waugh, *Chem. Phys. Lett.*, 1990, 171(5,6), 462-468.
- [144] L. J. Whitman, C. E. Barosch, W. Ho, *J. Chem. Phys.*, 1986, 85(6), 3688-3698.
- [145] / H. P. Bonzel, A. M. Bradshaw, G. Ertl, 57, Elsevier, Amsterdam, 1989, Vol. 57.
- [146] Z. Paál, G. Ertl, S. B. Lee, *Appl. Surf. Sci.*, 1981, 8, 231-249.
- [147] K. Altenburg, H. Bosch, J. Van Ommen, P. J. Gellings, *J. Catal.*, 1980, 66, 326-334.
- [148] G. Ertl, S. B. Lee, M. Weiss, *Surf. Sci.*, 1982, 114, 527-545.
- [149] A. Ozaki, K. Aika, Y. Morikawa, *Proc. 5th Intern. Congr. on Catalysis*, (Ed.: J. W. Hightower), North-Holland, Amsterdam, 1973, p. 1251.
- [150] G. Brodén, H. P. Bonzel, *Surf. Sci.*, 1979, 84, 106-120.
- [151] G. Pirug, G. Brodén, H. P. Bonzel, *Surf. Sci.*, 1980, 94, 323-338.
- [152] R. Schlögl, *Physics and Chemistry of Alkali Metal Adsorption*, (Eds.: H. P. Bonzel, A. M. Bradshaw, G. Ertl), Elsevier Science Publishers B. V. / Amsterdam, 1989, p. 347.
- [153] J. Norskov, *Physics and Chemistry of Alkali Metal Adsorption*, (Eds.: H. P. Bonzel, A. M. Bradshaw, G. Ertl), Elsevier, Amsterdam, 1989, p. 253.
- [154] N. D. Lang, S. Holloway, J. K. Norskov, *Surf. Sci.*, 1985, 150, 24-38.
- [155] G. Ertl, M. Huber, *Z. Phys. Chem. NF*, 1980, 119, 97-102.
- [156] D. R. Strongin, G. A. Somorjai, *J. Catal.*, 1988, 109, 51-60.
- [157] R. Kurzawa, K.-P. Kämper, W. Schmitt, G. Güntherodt, *Solid State Comm.*, 1986, 60, 777-780.
- [158] N. D. Shinn, *Phys. Rev. B*, 1990, 41, 9771-9782.
- [159] R. Schlögl, R. C. Schoonmaker, M. Muhler, G. Ertl, *Cat. Lett.*, 1988, 1, 237-242.
- [160] D. R. Strongin, G. A. Somorjai, *J. Catal.*, 1989, 118, 99-110.
- [161] M. Muhler, F. Rosowski, G. Ertl, *Catal. Lett.*, 1994, 24, 317-331.
- [162] B. Fastrup, *Frontiers in Catalysis: Ammonia Synthesis and Beyond*, (Eds.: H. Topsoe, M. Boudart, J. K. Norskov), J. C. Baltzer AG, Basel, 1994, Vol. 1, p. 273.
- [163] P. H. Emmett, S. Brunauer, *J. Am. Chem. Soc.*, 1933, 55, 1738-1742.
- [164] P. Stoltze, J. K. Norskov, *J. Catal.*, 1988, 110, 1-10.
- [165] S. Brunauer, K. S. Love, R. G. Keenan, *J. Amer. Chem. Soc.*, 1942, 64, 751-758.
- [166] M. Muhler, L. Pleth Nielsen, B. Fastrup, *Chem. Phys. Lett.*, 1991, 181, 380-382.
- [167] B. Fastrup, H. N. Nielsen, *Cat. Lett.*, 1992, 14, 233-239.
- [168] K. Kishi, M. W. Roberts, *Surf. Sci.*, 1977, 62, 252-266.
- [169] J. M. Thomas, R. Schlögl, *Angew. Chemie*, 1994, 106(3), 316-319.
- [170] K. Aika, A. Ozaki, *J. Catal.*, 1970, 16, 97-101.
- [171] J. Kubota, K.-I. Aika, *J. Phys. Chem.*, 1994, 98(44), 11293-11300.
- [172] Y. Izumi, K. Aika, *Chemistry Lett.*, 1995, 137-138.
- [173] Y. Izumi, K. Aika, *J. Phys. Chem.*, 1995, 99, 10346-10353.
- [174] Y. Izumi, K. Aika, *J. Phys. Chem.*, 1995, 99, 10336-10345.
- [175] K. Aika, T. Ohhata, A. Ozaki, *J. Catal.*, 1970, 19, 140-143.

- [176] J. Block, G. Schulz-Eckloff, *J. Catal.*, **1973**, *30*, 327-329.
- [177] P. H. Emmett, S. Brunauer, *J. Amer. Chem. Soc.*, **1933**, *55*, 1738-1739.
- [178] A. V. Hamza, G. D. Kubiak, R. H. Stulen, *Surf. Sci.*, **1990**, *237*, 35-52.
- [179] R. Brill, *J. Catal.*, **1970**, *16*, 16-19.
- [180] A. Ozaki, H. Taylor, *Proc. R. Soc. London A*, **1960**, *258*, 47-62.
- [181] A. Nielsen, J. Kjaer, B. Hansen, *J. Catal.*, **1964**, *3*, 68-79.
- [182] L. M. Aparicio, J. A. Dumesic, *Topics in Catalysis: Ammonia Synthesis and Beyond*, (Eds.: H. Topsoe, M. Boudart, J. K. Norskov), J. C. Baltzer AG, Basel, **1994**, Vol. 1 /, p. 233.
- [183] K. Aika, A. Ozaki, *J. Catal.*, **1970**, *19*, 350-352.
- [184] P. Stoltze, J. K. Norskov, *Phys. Rev. Lett.*, **1985**, *55*(22), 2502.
- [185] P. Stoltze, J. K. Norskov, *Topics in Catalysis: Ammonia Synthesis and Beyond*, (Eds.: H. Topsoe, M. Boudart, J. K. Norskov), J. C. Baltzer AG, Basel, **1994**, Vol. 1, p. 253.
- [186] P. Stoltze, H. Topsoe, *Ammonia: Catalysis and Manufacture*, (Ed.: A. Nielsen), Springer Verlag, Berlin, **1995**, Vol. / 2, p. 21.
- [187] M. Bowker, *Cat. Today*, **1992**, *12*, 153-163.
- [188] M. Bowker, I. B. Parker, K. C. Waugh, *Appl. Catal.*, **1985**, *14*, 101-118.
- [189] M. Bowker, I. Parker, K. C. Waugh, *Surf. Sci.*, **1988**, *197*, L223-L229.
- [190] G. Ertl, *J. Vac. Sci. Technol. A*, **1983**, *1*, 1247-1253.
- [191] P. Stoltze, J. K. Norskov, *Surf. Sci.*, **1988**, *197*, L230-L232.
- [192] J. K. Norskov, P. Stoltze, *Surf. Sci.*, **1987**, *189/190*, 91-105.
- [193] J. A. Dumesic, A. A. Treviño, *J. Catal.*, **1989**, *116*, 119-129.
- [194] G. Haase, M. Asscher, R. Kosloff, *J. Chem. Phys.*, **1989**, *90*(6), 3346-3355.
- [195] J. J. F. Scholten, P. Zwietering, J. A. Konvalinka, J. H. De Boer, *Trans. Faraday Soc.*, **1959**, *55*, 2166.
- [196] P.R. Watson, M.A. van Hove, K. Hermann, , NIST Standard Reference Data Program , Gaithersburg, **1995**.